Powder Technology 449 (2025) 120393

Contents lists available at ScienceDirect

Powder Technology

journal homepage: www.journals.elsevier.com/powder-technology

Review

Powder spreading and spreadability in powder-based additive manufacturing: State of the art and perspectives

Wenguang Nan [a,b,*], Lanzhou Ge [a], Ziming He [a], Zhonggang Sun [c], Jinzhong Lu [d]

[a] School of Mechanical and Power Engineering, Nanjing Tech University, Nanjing 211816, China
[b] School of Chemical and Process Engineering, University of Leeds, Leeds LS2 9JT, UK
[c] College of Materials Science and Engineering, Nanjing Tech University, Nanjing 211816, China
[d] School of Mechanical Engineering, Jiangsu University, Zhenjiang 212013, China

GRAPHICAL ABSTRACT

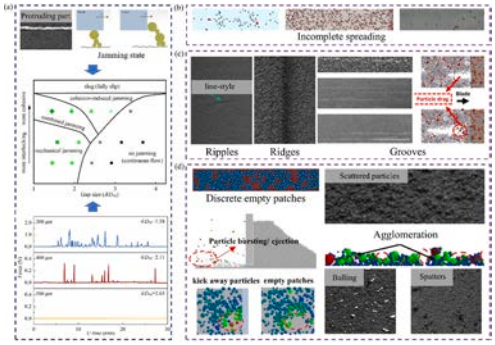

ARTICLE INFO

Keywords:
Additive manufacturing
Powder spreading
Spreadability
Defects
Machine learning

ABSTRACT

Powder-based additive manufacturing (AM) technology has been widely used in various industries. The powder spreading process and its spreadability play a crucial role in ensuring the quality of the final product and the overall production system. This review aims to provide a comprehensive understanding of the issues related to powder spreading and spreadability in AM, as they significantly impact production consistency, process optimisation, and manufacturing cost reduction. A clear definition of spreadability and its corresponding metrics are presented, and the difference between the spreadability and flowability is also clarified. Meanwhile, the factors influencing the spreadability and spreading process, including the powder mixture and gas atmosphere, are thoroughly reviewed. The underlying mechanisms of these factors are discussed and summarised, particularly the critical spreading speed and the shear band developed in front of the spreader. Furthermore, the defects within the spread layer are carefully classified with a summary of the corresponding causes and mechanisms, in which the importance of particle jamming is clarified. The detection of defects using machine learning and the optimisation of spreadability are also reviewed. Finally, future trends and research opportunities, such as the integration of artificial intelligence into in-situ defect detection and subsequent adjustment of spreading conditions, are highlighted.

* Corresponding author at: School of Mechanical and Power Engineering, Nanjing Tech University, Nanjing 211816, China.
E-mail address: nanwg@njtech.edu.cn (W. Nan).

https://doi.org/10.1016/j.powtec.2024.120393
Received 13 May 2024; Received in revised form 25 September 2024; Accepted 21 October 2024
Available online 24 October 2024

1. Introduction

Additive manufacturing technology stands at the forefront of innovation, rapidly evolving to become a cornerstone across various high-tech industries such as aerospace, pharmaceuticals, and equipment manufacturing [1–3]. Among its diverse methodologies, powder-based additive manufacturing emerges as a pivotal player, exemplified by techniques like laser powder bed fusion (LPBF) and binder jetting 3D printing [4–8]. This approach utilizes diverse powders as foundational materials, undergoing a series of steps involving spreading, melting, and solidification to produce the desired products. The powders employed in this technique are usually fine and cohesive. However, these powders present formidable challenges during the spreading process, where a powder heap is spread onto a work surface using a blade or roller spreader to create a thin powder layer. Meanwhile, the spreading process involves complex flow dynamics within confined spaces, heavily influenced by friction and transient jamming arising from interactions with solid boundaries. The inconsistencies of the spread layer such as empty patches or uneven packing are usually inevitable during the powder spreading process, which detrimentally impacts the quality of the final manufactured component, leading to flaws like pores and cracks [9]. Hence, a profound comprehension of the physical and mechanical attributes of powders and spreading conditions that influence their spreadability and spreading process is valuable for technological advancement. This understanding facilitates the seamless integration of novel materials, enhances product quality, optimizes manufacturing processes, and ensures a coherent workflow throughout.

The powder spreading process has been reviewed by Sehhat et al. [10], Capozzi et al. [11], and Miao et al. [12], giving a general understanding of the spreading process and quality of spread layer. Sehhat et al. [10] did a brief review on the previous work performed on spreadability metrics, in which the impact of spreading process parameters and powder characteristics were involved. However, the corresponding mechanisms of spreading process were also not detailed discussed. The spreadability was not well defined in their review, and the involving powder dynamic repose angle and powder mass flowrate into the spreadability might induce some confusion. Capozzi et al. [11] reviewed different spreading systems, in which the experiment rigs and testing tools were focused. Miao et al. [12] further provided a detailed literature review on powder spreading, mainly focusing on the effects of influencing factors on the quality of spread layer in terms of density and surface condition of the spread layer. Three groups of influencing factors were discussed in their review, including spreaders, spreading parameters, and feedstock powder properties.

Based on recent articles and current reviews of the powder spreading process, this article offers a clear definition of spreadability. The corresponding metrics are thoroughly reviewed, including empty patches, packing density, and surface roughness, with detailed calculation methods provided. Additionally, the article clearly distinguishes between spreadability and flowability. Meanwhile, the factors influencing the spreadability and spreading process are comprehensively explored, encompassing spreading conditions and particle properties, in which the mixture of different types of powder is also focused. The impact of gas atmosphere, especially for fine powder at high spreading speed, is highlighted. The underlying mechanisms of these factors are discussed and summarised, in which the critical spreading speed and the formation of shear band in front of the spreader are involved. The characterisation of particle properties at the level of single particle is also examined. Moreover, the defects within the spread layer are classified, with corresponding causes and mechanisms summarised, in which the significance of particle jamming is clarified. The detection of defects using machine learning, such as conventional neural network (CNN), as well as the methods of avoiding the defects and optimising the spreadability, are also reviewed. Finally, attention is given to future trends and research opportunities, particularly the optimisation of spreadability of extremely fine powder through spreader geometry and vibration conditions and the application of artificial intelligence (AI) into the in-situ defects detection and auto-adjustment of spreading conditions. This

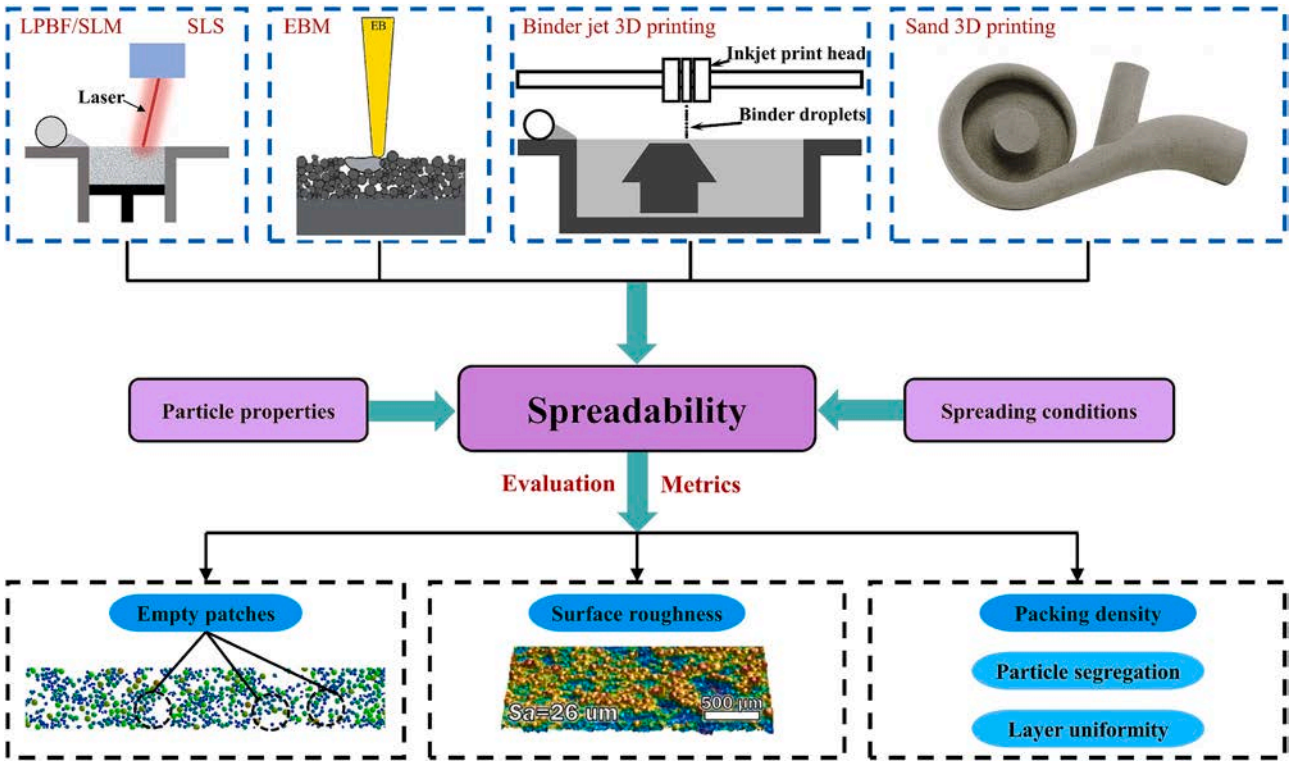

Fig. 1. Framework of spreadability and the corresponding evaluation metrics, in which the snapshots of empty patches from Nan et al. (2018) and surface roughness from Yim et al. (2022) are used.

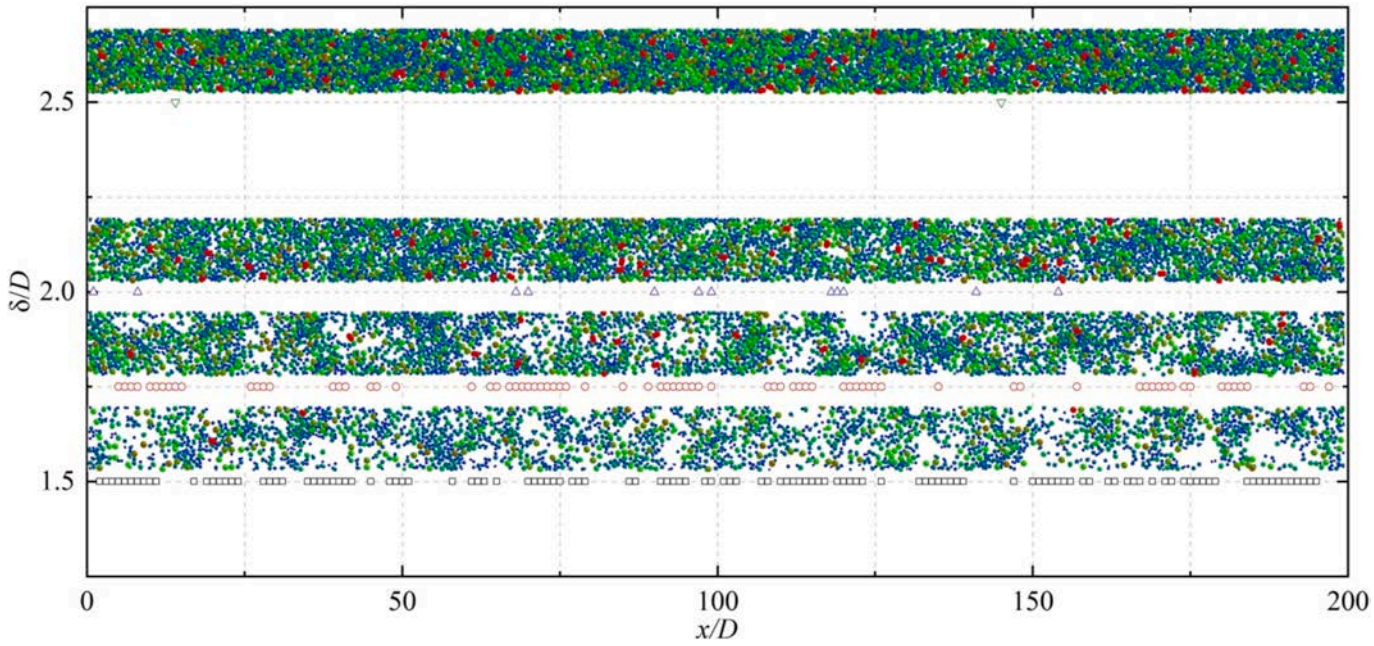

Fig. 2. Empty patches along the spreading direction as simulated by Nan et al. (2018), in which x is the position in direction of powder spreading, D is the particle diameter, δ is the gap height, every legend underneath each snapshot indicates that there is at least one empty patch in the Y direction, and connected legends with no breaks between them are considered to belong to the same empty patch.

review not only enhances the understanding of the fundamental mechanisms of the spreadability and spreading process, but also provides practical guidance for the operation of real manufacturing processes.

2. Metrics of spreadability

The spreadability is a complex feature of powder, as it is obviously influenced by the particle properties and spreading conditions. It could be generally defined as the ability of a feedstock material to be spread out in layers that fulfil the requirements for the AM process [13]. It can also be defined as the ability to transform bulk powder using a spreader into a thin and uniform layer with a thickness of a few multiples of particle size, without the formation of empty patches and agglomerates and the presence of rough surface, according to the work of Nan and Ghadiri [14–17]. Good spreadability usually results in a thin particle spread layer that is dense and uniform, i.e. a uniform surface texture, a desired layer density and layer thickness, little change in the distributions of particle size and particle shape, an absence of defects. It is strongly influenced by powder flow behaviour in the narrow gap between the spreader and the base, where transient jamming due to mechanical and/or cohesive arching readily occurs. As shown in Fig. 1, the diversity of powder properties and the sensitivity to spreading conditions make the evaluation and prediction of spreadability challenging, but highly desirable. The spreadability could be estimated and examined through the empty patches, surface roughness, packing density, particle segregation or layer uniformity, etc. Particle segregation in terms of the deviation of particle size and particle shape from the original powder material is usually not easy to obtain for a thin spread layer in the experiments and AM machines, as an accurate and quick sampling is challenged for a thin layer of powder [18]. Layer uniformity is an alternative method and can be post-calculated based on the packing density or surface roughness at local regions. Thus, the first three metrics are discussed and reviewed here, including empty patches, surface roughness and packing density. It should be noted that not all metrics are needed to be collected to assess the powder spreadability or compare the spreadability of different powder materials.

2.1. Empty patches

The empty patches refer to the regions on the work surface, that are not covered by enough powder or particles. The size of the empty patches could range from a few of particle diameter to a few of millimetres or even centimetres, depending on the particle properties and spreading conditions. This concept is used by Nan et al. [14], Ahemd et al. [16] and Shaheen et al. [19]. It is also called "vacancy" in Chen et al. [20] and Han et al. [21], "void" in Tan et al. [22], Gatta et al. [23], Yim et al. [24] and Lampitella et al. [25], "cavity" in Marchais et al. [26] and Si et al. [27,28]. It induces significant defects within the spread layer and poses great challenges for the spreading process. Therefore, the characterisation and detection of empty patches are essential for quantifying the spreadability. As it can be quickly examined through image analysis of the spread layer, it is also the simplest way to in-situ characterise the spreadability.

Nan et al. [14] characterised empty patches by their size and frequency distribution based on the spatial distribution of particles within the spread layer. In their cases, the spread layer was divided into several bins, and an individual bin was assumed to be an empty patch if its particle fraction met the following criterion:

$$\frac{\sum V_P}{\Delta x \times \Delta y \times (\delta - \delta_c)} < 0.1 \tag{1}$$

where V_p is the volume of an individual particle within the bin; $\delta_c = 1.0D_{90}$ is the critical gap; Δx and Δy are the sizes of the bins in X and Y directions, respectively; and δ is the gap height, i.e. the distance between the work surface and the bottom surface of the spreader. The distribution of empty patches along the spreading direction (i.e. the X direction) in their work is shown in Fig. 2, where every legend underneath each δ/D_{90} snapshot indicated that there was at least one empty patch in the Y direction. The connected legends, i.e. those with no breaks between them, are considered to belong to the same empty patch. By accounting the number and position of the legends, the size distribution and frequency of the empty patches could be obtained.

This method was further followed by the experimental work of Ahmed et al. [16]. They proposed a simple and quick method to assess

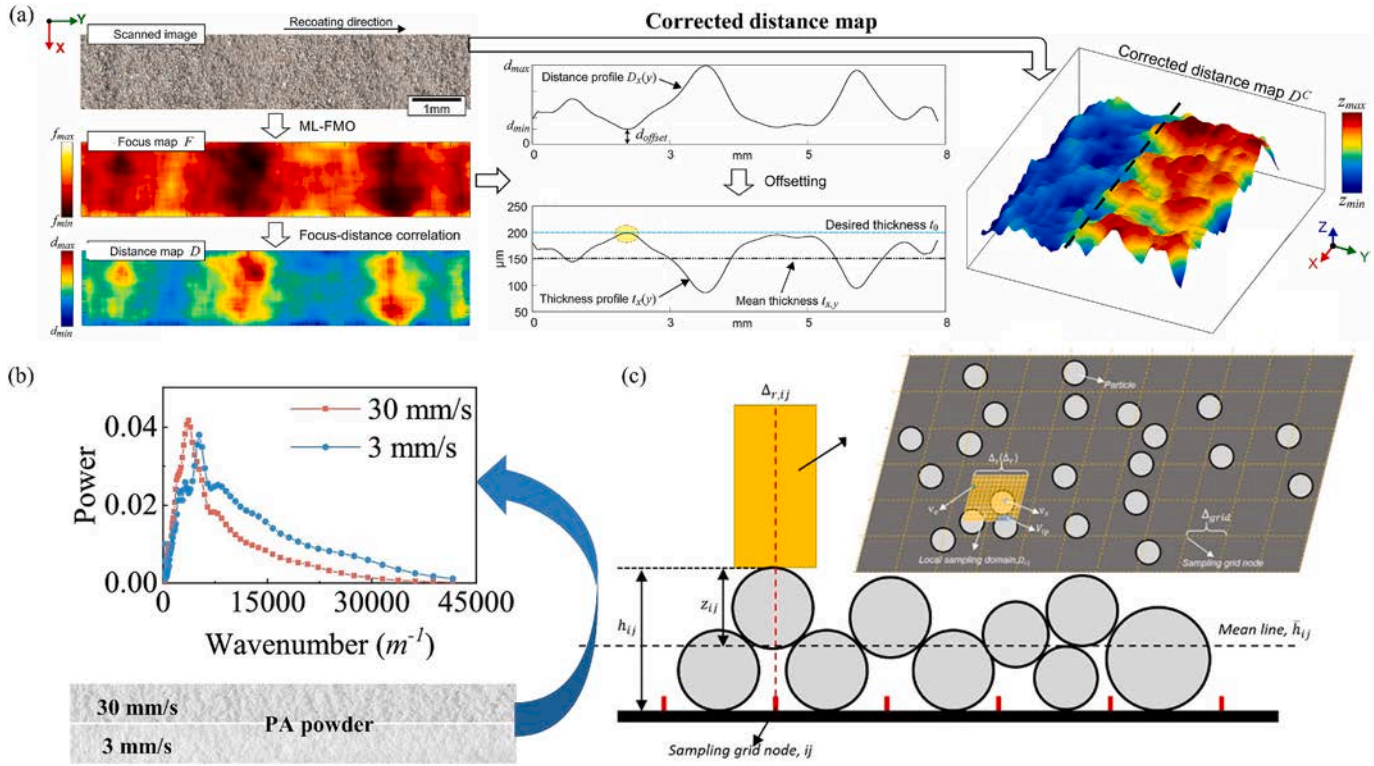

Fig. 3. Characterisation of the surface roughness of the spread layer: (a) in-situ scan technique developed by *Le* et al. (2021); (b) camera-based technique with wavelet power spectrum analysis developed by Lupo et al. (2023); (c) 2D Cartesian sampling method developed by He et al. (2020) for DEM simulation.

the spreadability of 316 L stainless steel powder based on 2D image analysis. A Stanton cutter blade was cut along its length by laser to create a gap in the middle. Five depths of cut in the range of 45–135 μm were used, corresponding to different gap heights or layer thickness. To provide a fully rough base, abrasive Emery papers were used as the work surface. For the analysis of the empty patches, they provided the details step by step, including image processing through the MATLAB and ImageJ software packages. The spread layer was reconstructed by several segmented SEM images, and the regions meeting the following criterion were deemed as empty patches.

$$\frac{\sum A_p}{\Delta x \times \Delta y} \leq 0.3 \tag{2}$$

where A_p is the area occupied by the particles.

For powders with poor spreadability, large empty patches could be formed during the spreading process. Thus, empty patches could also be used for quick and quantitative comparison of spreadability through naked-eye observation of the morphology of the spread layer. For example, Cordova et al. [29] experimentally identified different kinds of empty patches in the spread layer, i.e. deep lines and areas without particles caused by unexpected pause in the movement of spreader, long lines due to larger particles or agglomeration of particles blocking/jamming the gap.

2.2. Surface roughness

The surface roughness of the spread layer is adopted by many researchers to estimate the spreadability, and several characterisation methods have been proposed for both experiments and simulations. The methods used in the experiments are mainly based on image scanning of the spread layer, using confocal laser scanning microscopy (CLSM) [20,30–33], computed tomography (CT) [31], and in-house tools developed based on digital cameras [34]. Based on the CLSM technique, Chen et al. [20,30] measured and compared the layer profile and surface roughness of the spread layer at different spreading speeds for PA12 powder and Hastelloy-X alloy powder. In particular, Beitz et al. [31] investigated the surface roughness of the spread layer of PA12 powder by using CLSM and X-ray micro-CT techniques. They showed that the surface roughness obtained from the latter was less accurate and had a lower average value than that obtained using CLSM. By using a digital camera with a microscope at 10× magnification, Lupo et al. [34] developed a new method to characterise the surface roughness, as shown in Fig. 3. A time-averaged wavelet power spectrum analysis was carried out for the image of the spread layer using the "Wavelet Toolbox" in MATLAB, and a quantitative parameter based on the wavenumber of peaks was used as the indicator related to the surface roughness. Recently, by equipping the spreader with a contact image sensor (CIS) unit taken from a Canon LiDE 220 flatbed scanner, *Le* et al. [35] developed a new and in-situ scan technology, and an example is illustrated in Fig. 3. First, the spread layer was scanned from the CIS, and then a focus map was generated from the scanned image by using a modified Laplacian focus measure operator (ML-FMO). By applying a focus-to-distance conversion function, a distance map D(x, y) was generated based on the focus map. Surface roughness could be estimated from the thickness profile or corrected distance map through the analysis of D(x,y).

On the other hand, the surface roughness could also be obtained based on the spatial position of particles within the spread layer, which is usually used in the modelling of spreadability and spreading process using Discrete Element Method (DEM). Haeri et al. [36] used a ray-tracing technique, i.e. 10 rows of light sources were applied in the spreading direction, with 500 equally distanced sources used in the Y direction for each row, resulting in 5000 data points in total. Each ray intersected the bed at a specific height h, and the standard deviation of h normalised by the particle size was defined as the surface roughness of the spread layer. Moreover, He et al. [37] provided a detailed calculation of surface roughness based on the height of the spread layer with the aid of a 2D Cartesian grid. They calculated the maximum Z coordinate

within each local sampling grid, as shown in Fig. 3, and then calculated the arithmetical mean deviation as the surface roughness. Similarly, Parteli et al. [38] calculated the standard deviation of the height profile of the spread layer, i.e. the upper boundary of the surface of the spread layer projected on the xz plane (x is the spreading direction, and z is the vertical direction). These techniques have also been followed and used in other studies [39,40].

2.3. Packing density

The packing density is one of the most direct methods for evaluating spreadability. It can be calculated for the whole spread layer or local regions of the spread layer. Local packing density could be further post-calculated as layer uniformity or powder bed density homogeneity [41]. In traditional definition, packing density is referred to the powder bed mass divided by the volume it occupies. However, for the thin spread layer in AM, its volume is not well defined. Generally, the packing density of the spread layer could be normalised as:

$$\psi = \frac{M}{\rho A \lambda} \tag{3}$$

where M and A are the total mass of particles and area for the spread layer or local regions of interest, respectively; ρ is the density of the material of the particle; and λ is a parameter, which varies in different works. For example, λ = gap height in Wischeropp et al. [6], λ = number-based particle size D_{90} in Nan et al. [14], and λ = height of the spread layer measured from an optical 3D microscope in Wu et al. [42]. In particular, He et al. [37] proposed a novel digital-based method using a cartesian grid to calculate the local packing density in their DEM simulation, where the domain with the same area as the spread layer and the same height as the gap (i.e. λ = gap height) was discretised into voxels. The voxels located within the particles were then labelled as solid voxels, and the packing fraction was simply determined as the ratio of the number of solid voxels to the total number of voxels within the local sampling domain. Similar methods have also been used by other researchers, such as Zhang et al. [43], Cao et al. [44] and Si et al. [27]. Furthermore, Mehrabi et al. [45] defined spreadability as the ability to spread powder from a reservoir (e.g. hopper or heap) to a surface (or in a space) with the same packing fraction as the reservoir. Thus, the spreadability in their work was calculated as the ratio of the packing density of the spread layer to that in the reservoir [46], given as:

$$\widehat{\psi} = \frac{\rho_{layer}}{\rho_{reservoir}} \tag{4}$$

It should be noted that this definition may cause arguments, as it is not directly linked to the demand of the powder spreading process in AM. For example, for the powder with strong cohesion or very irregular particle shape, the packing density in the reservoir would be very low, and the spreadability in Eq. (4) may result in a paradox that this kind of powder has a better spreadability than the powder with spherical particle shape and slight cohesion, but the latter usually could produce a better quality of spread layer. Meanwhile, although the packing density of the whole spread layer is not emphasised by ASTM F3522–22 [41] (i.e. "found to not strongly influence part density, although there will be a limit where low bed density will influence mechanical properties negatively"), it is critical for very cohesive powder, especially in binder jet 3D printing, which may create problems for the successful manufacturing of the product.

3. Spreadability and flowability

Spreadability and flowability are two different measures of powder flow characteristics, albeit inter-related, as presented by Nan and Ghadiri [14–16,47]. They thought that the spreadability is strongly affected by the solid boundaries, i.e. particles are sheared as they flow through a narrow gap, and particle jamming makes the spreadability different from the flowability. Spreadability is the ability to transform bulk powder into a thin uniform layer, while flowability is a measure of the ease with which bulk powder flows. They differ in that flowability gauges resistance in naturally-developing shear bands, whereas spreadability concerns flow within confined spaces, heavily influenced by friction and transient jamming due to interactions with confining solid boundaries [48]. Similar points have also been clarified by Cordova et al. [29], Yim et al. [40], Lupo et al. [34], Mehrabi et al. [45] and Ajabshir et al. [49]. For example, Cordova et al. [29] found that the flowability tested by Hall flow tester is inconsistent with the spreadability characterised by the packing density. Yim et al. [40] found that the static and dynamic repose angles of powder could not represent the spreadability characterised by surface roughness. Lupo et al. [34] experimentally analysed the surface roughness of the spread layer of four polymer powders, and their results showed that the flowability and spreadability of these four powders were not consistent. Recently, for metal powder used in binder jet 3D printing technology, Nan et al. [48] found that employing bulk characterisation tests, such as shear cell tests and compressibility indices, resulting in contradictory outcomes, as shown in Table 1, while the spreadability data derived from the DEM simulations did not exhibit a strong correlation with the results obtained from the characterisation of bulk powder.

The main difference between the spreadability and flowability in terms of features is that the spreadability is sensitive to the size effect and particle jamming. The spreadability is sensitive to the relative size

Table 1
Flow classification of two kinds of gas-atomised 316 L stainless steel powder used in binder jet 3D printing, as measured by Nan et al. (2024) using various commercial tools.

Methods	Samples	Not flowing	Very cohesive	Cohesive	Easy flowing
Shear Cell assessment	Sandvik	–	√	√	–
	Ancor	–	–	√	√
Compressibility index and Hausner ratio	Sandvik	–	–	–	√
	Ancor	–	–	–	√
Hall Flow Tester and Carney Flow Tester	Sandvik	√	–	–	–
	Ancor	√	–	–	–
Static angle of repose	Sandvik	Poor flowing (repose angle of 51°)			
	Ancor	Moderate flowing (repose angle of 39°)			

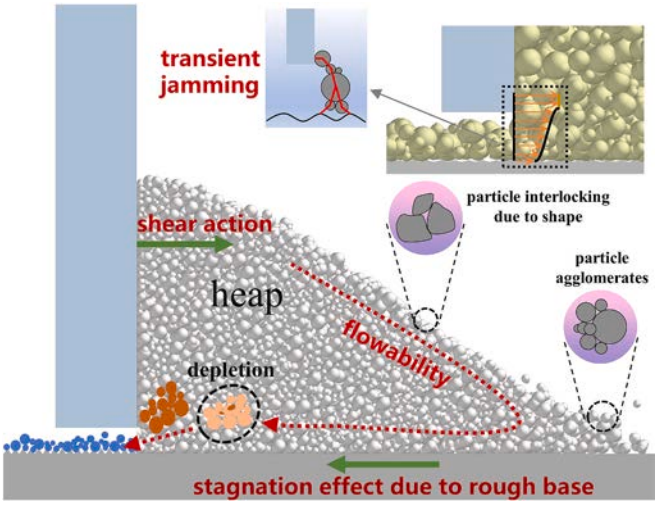

Fig. 4. Illustration of the mechanisms of the spreading of particles from the heap onto the rough base at single-particle scale as reported by Xu et al. (2023).

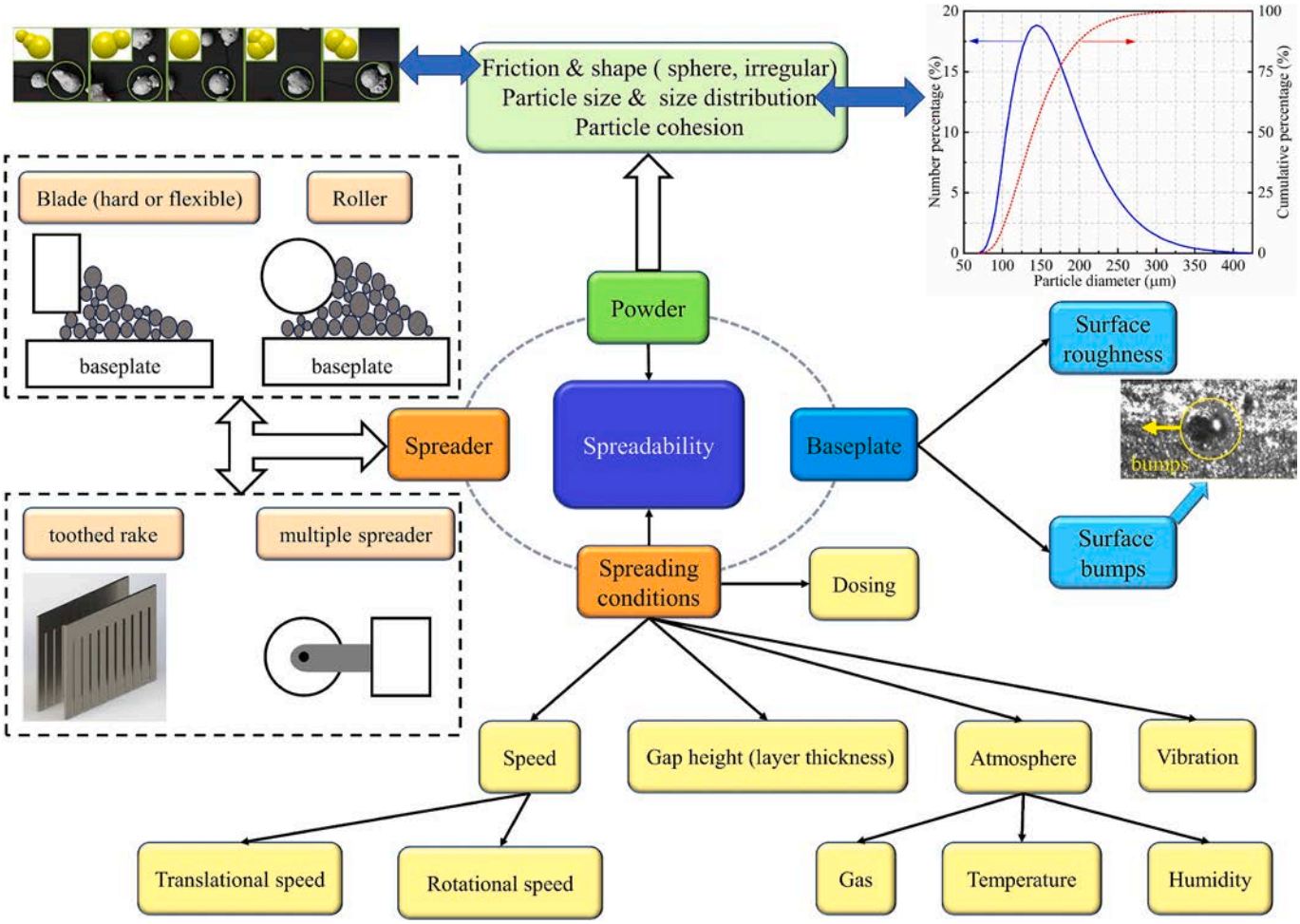

Fig. 5. A summary of factors affecting the spreadability.

between the gap height (or layer thickness) and the particle size, which is an intrinsic characteristic of powder spreading. It demonstrates that the relative powder spreadability should be compared at the same ratio of the gap height to the particle size, especially for powders with different particle size classes, as suggested by Nan et al. [14] and Xu et al. [17]. Of course, if the powders are in a similar size range, for simplification, the gap height could also be directly used without normalisation by the particle size. Meanwhile, as an important feature, particle jamming makes powder spreadability significantly different from powder flowability. As shown in Fig. 4, besides particle detaching from the main heap and re-filling/circulation within the heap, the process of particles transforming from the bulk heap to form a thin spread layer is significantly affected by transient jamming near the gap. Of course, flowability also has effects on the jamming itself, as shown by Nan et al. [48], in which the particles would also be jammed due to strong cohesion between particles if the flowability was very poor. The jamming behaviour not only transiently suspends the particle flow through the gap, but also leads to special particle phenomena, such as particle dragging and particle bursting/ejection, which further make the spreadability different from the flowability. Therefore, it is helpful to set the gap height as a multiple of D_{90} by number, as this characteristic of the particle size distribution accounts for transient jamming, which adversely affects the quality of the spread layer.

As spreadability and flowability are 'siblings', related by their 'DNA'. Meanwhile, the re-filling circulation of particles within the heap is dominated by the effect of powder flowability, as shown in Fig. 4. Thus, although powder spreadability is not directly related to powder flowability, spreadability is significantly affected by flowability to some extent. The spreadability of powder with good flowability is usually not poor. Nan et al. [47] clarified that in order to gain a better spreadability, the power should not be too free flowing, and the power with slight cohesion or interlocking due to the particle shape was more attractive. Similarly, Vakifahmetoglu et al. [50] reported that when the flowability was neither too high nor too low but allowed optimum spreading, a high spreadability could be obtained.

Considering the fact that there are limited commercial instruments available to date for assessing the powder spreadability, the tests based on traditionally commercial or newly-developed instruments are still attractive to provide useful information to infer the spreadability of powders used in AM, such as dynamic repose angle and cohesive index from GranuDrum instrument, specific flow energy from FT4 rheometer, unconfined yield strength and internal angle of friction from shear cell. Recently, several researchers [51–54] have attempted to characterise the flowability of AM powder and hoped to determine its spreadability. For example, Espiritu et al. [52] characterised the flowability of IN625 and Ti6Al4V powder used in laser powder bed fusion (LPBF) and electron beam melting (EBM) by using the dynamic repose angle and cohesive index from Granudrum, and their results highlighted the effects of atmospheric (air/argon) and low-pressure environments on flowability. Nan et al. [48] demonstrated that Ball Indentation Method [55] could emerge as a more discriminative technique to characterise the spreadability to some extent, effectively distinguishing the flow resistances exhibited by different powder samples, particularly at low stress levels experienced by the powders during an additive manufacturing spreading process. Furthermore, if we need to obtain a comprehensive characterisation of spreadability, experimental

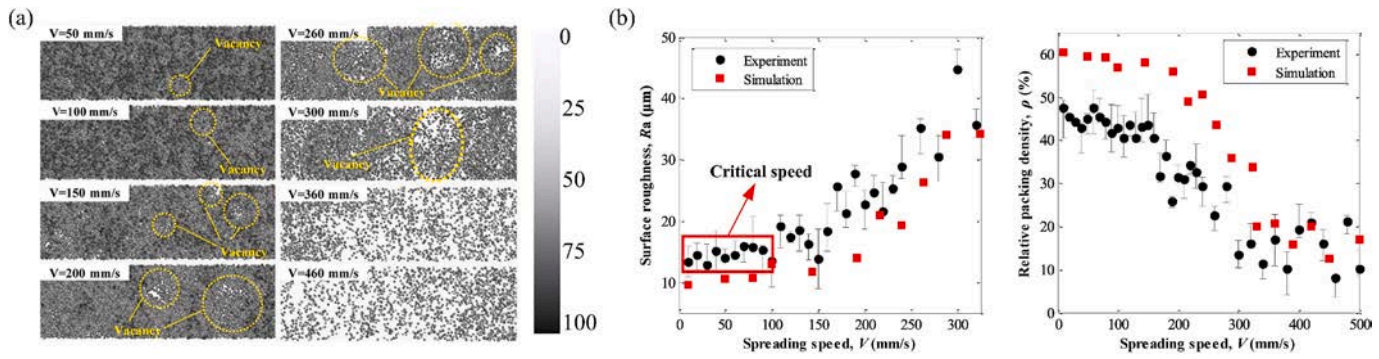

Fig. 6. Effects of blade speed on the spreadability as reported by Chen et al. (2020): (a) snapshots of the spread layer, in which V is the spreading speed, with the same meaning as U; (b) surface roughness and relative packing density of the spread layer.

characterisation of the physical and mechanical properties of single particle and numerical characterisation using DEM modelling are also necessary, in which artificial roughness must be imposed on the base by using clumped cylinders or spheres, or directedly reconstructing from scanning the solidified layer manufactured in AM machine. On the other hand, for the instruments specified for spreadability developed in the future, the gap size used in characterisation tests should be limited to a few of particle size, and the roughness of the base should be taken into account by using an abrasive paper or a plate with specified roughness.

4. Effects of spreading conditions

The spreadability is significantly affected by the spreading conditions, as detailed shown in Fig. 5. The spreading conditions include the speed of the spreader, the gap height, the surface features of the base plate, and the atmosphere. The gap height is also called layer thickness in some research. For most commercial AM machines, the spreader is usually a blade or a roller. Here, the blade spreading system is first focused, and then the roller spreading system is reviewed and compared with the blade spreading system, in which the underlying mechanisms are highlighted.

4.1. Effect of spreading speed in blade spreading system

The spreading speed has a significant influence on the spreadability. In most situations, too high of a spreading speed can induce a high probability of forming empty patches, low packing density and large surface roughness, resulting in a decrease in the quality of the spread layer. The underlying mechanism is the shear action of the blade spreader, which is related to the dilation effect and the drag effect of the particles in front of the blade. However, too low of a spreading speed would lead to a low efficiency of the spreading process in the AM machine, which is not intuitively expected. Nan et al. [56] analysed the critical and optimum spreading speed by comparing two timescales, i.e. the gravity inertial timescale $t_g = (D_{90}/g)^{1/2}$ and the spreading inertial timescale $t_s = D_{90}/U$. The first is the time taken by a particle with zero initial velocity to fall a distance of $D_{90}/2$ under gravity acceleration g, while the latter is the time taken by the blade with velocity U to pass over a static particle with D_{90}. If the spreading inertial timescale is much less than the gravity inertial timescale, i.e. $t_s = t_g/k$ ($k >> 1$), the gravity effect on the spreading process could be limited, and the particles do not have enough time to fall down to fill the dilated zone caused by blade shearing. In this concept, the critical spreading speed is given as:

$$U_c = k\sqrt{gD_{90}} \tag{5}$$

In their work, the critical speed was approximately 0.1 m/s with $k = 5$, where 316 L stainless powder with a number-based D_{90} of 45 μm was used. This value was further validated by Yao et al. [3] through DEM simulation. As shown in Fig. 6, the experiments of Chen et al. [57] also validated the existence of a critical speed, which was approximately 0.1 m/s. Similarly, Wang et al. [58] also thought that there was a critical spreading speed, although the value was not provided in their work.

Following the above concepts, the effects of the spreading speed on the spreadability are summarised in Nan et al. [47], Xu et al. [17], Yao et al. [3,59,60], and Chen et al. [20]: 1) stronger dilation effects: the particles could not have enough time to fill the depletion zone caused by the particles entering the gap zone, resulting in fewer particles being able to enter the gap region; 2) more inertial effects of the particles during the deposition process: too large spreading speed could outcome the stagnation effect of the rough baseplate, and thus reduce the difference between the particle velocity and blade speed, resulting in fewer particles leaving away from the blade, which is also called dragging effect. Therefore, the spreading speed usually has negative effects on the spreadability. For example, Lee et al. [61] concluded that a higher blade speed may produce poor surface uniformity based on top-viewed images of the spread layer. They also found that the size distribution of particles within the spread layer would shift to finer particles with the increase of spreading speed. Si et al. [27] investigated the effects of the spreading speed on the layer quality and particle dynamics, and they found that with the increase of spreading speed, the packing density decreased while the average particle velocity increased. A negative correlation between spreadability and spreading speed is also found in Gatta et al. [23], Yim et al. [24], Marchais et al. [26] and other articles [3,49,59,60,62–69]. It should be noted that above perspectives are also applicable for blades with other shapes. For example, Lampetella et al. [25] simulated the spreading process of a U-shaped blade, and their results showed that with the increase of spreading speed, the packing density and thickness of the spread layer decreased, resulting in worse spreadability.

4.2. Effect of gap height in blade spreading system

A large gap height usually leads to good layer quality, but it is limited by the manufacturing resolution required by the AM machine. It should be noted that due to the asperities and defects of the work surface formed by the sintering of the previous spread layer, the local gap height between the blade bottom and the work surface is actually not constant and varies along the spreading direction. Nan et al. [14] explored the mechanism of the effects of gap height on the spreading process in terms of the particle velocity around blade and empty patches formed in the spread layer. They found that a larger gap height would improve the quality of the spread layer, due to the reduction of the jamming and dragging effects of the particles underneath the blade, as indicated by the shear band shown in Fig. 7. They [47,56] also found that a narrow gap would result in particle segregation within the spread layer due to particle jamming. Similarly, Si et al. [27] claimed that poor packing density and surface uniformity in narrow gaps were the results of particle blocking/jamming. Therefore, it demonstrates that setting the gap

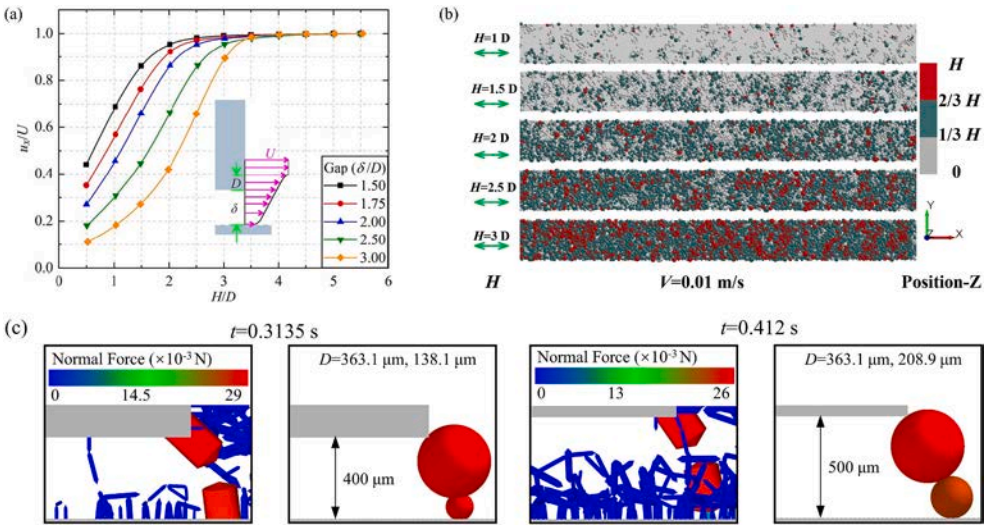

Fig. 7. Effects of gap height on the spreading process: (a) dragging effects indicated by the shear band as proposed by Nan et al. (2018), in which u_x is the averaged velocity of particles in the spreading direction, U is the spreading speed, δ is the gap height, D is the particle diameter, and H is the averaged position of particles; (b) snapshots of the spread layer as obtained by Yao et al. (2021), in which H is the gap height, with the same meaning as δ, and V is the spreading speed, with the same meaning as U; (c) snapshots of the force chain and jammed particles as observed by Xu et al. (2024).

Table 2
Corresponding parameters of some research of roller spreading system.

Powder	Particle size (μm)	Roller diameter (mm)	Translational speed (mm/s)	Rotational speed	References
PA12	D_{50} = 58	2.5	20–180	165 rpm	Parteli et al. (2016) sim
316 L	D_{90} = 45	4	80	60 rad/s	Nan et al. (2020) sim
316 L	D_{90} = 45	2	80	0–200 rad/s	Nan et al. (2020) sim
Al_2O3	D_{50} = 48	3–8	40–160	40–320 rpm	Zhang et al. (2020) sim
316 L	D = 5–55	10	10–500	60 rpm	Chen et al. (2020) exp
Hastelloy X Alloy	D_{50} = 34	2	50	6000 rpm	Wang et al. (2020) sim
PA12	D = 20–140	10	50–300	10–60 rad/s	Tan et al. (2021) sim
PA12	D = 30–70	10	50–150	0–144 rpm	Cheng et al. (2022) sim
Al_2O_3	D_{50} = 22, 49, 46	20	5–50	0–300 rpm	Oropeza et al. (2022) exp
Ti6Al4V	D_{50} = 34	0.6	20	0	Li et al. (2023) sim
Al_2O_3	D_{50} = 55	5	100	200 rpm	Zhang et al. (2023) sim
Ti6Al4V	D_{90} = 16, 19, 30	10	5–50	0–500 rpm	Penny et al. (2023) exp

height as a multiple of D_{90} by number would be helpful as it is accountable for the features of jamming.

Chen et al. [70] proposed that static and dynamic wall effects were the main mechanisms for the effects of gap height on the packing density of the spread layer, which was also followed by Meier et al. [62] and Yao et al. [60]. Meier et al. [62] found that higher gap would contribute to a greater packing density, owing to the combination of more space for particle rearrangement and a decreased static wall effect. Yao et al. [60] conducted a comprehensive study on the variation of spreadability under different gap heights through the structure uniformity and relative volume fraction of the spread layer. They considered that when the gap increased, the wall effects and probability of forming force arches (i.e. ring-shaped strong force chain network, creating localised areas of high stress and hindering smooth flow of particles, as shown in Fig. 7(c) and indicated on the transient jamming snapshot as red chain of forces in Fig. 4) would be reduced, and thus the quality of the spread layer was improved, as shown in Fig. 7. Other research [21,23,58–60,63,64,68,71] also showed that the quality of the spread layer could be increased by larger gap height, in which various mechanisms have been proposed to explain this effect. However, the underlying mechanism of the effect of gap height on spreadability could be summarised as dragging effects indicated by the shear band of granular flow, particle jamming, and wall effects, although they maybe interrelated.

4.3. *Effect of spreading conditions in roller spreading system*

Compared to the blade spreading system, the system using a roller introduces rotational action on the heap, with two additional parameters, i.e. the rotational speed and diameter of the roller, for which some examples are listed in Table 2. Compared to the blade spreading system, the main difference of roller spreading is the convection and circulation of particles occurring in the heap (i.e. particles are lifted up by the roller and then cascade down on the heap slope before they are collected by the gap), due to the cascading style distribution of the particle velocity, as observed by Nan et al. [72] and shown in Fig. 8. The convection and circulation of particles would make it more difficult for them to enter the gap region but easier to fill the depletion region, resulting in a stronger dragging effect and less dilation effects. The circulation and convection of particles also cause the particles to have more time to rearrange, resulting in a higher density of the heap (fine particles filling the voids between coarse particles) but also larger potential for particle segregation. These features make the flow behaviour of particles much different from that of a blade spreading system. Meanwhile, the geometry of the roller itself could result in a large contact area between the heap and spreader, providing larger normal force and compaction effect on the heap, as reported by Zhang et al. [73].

Due to these mechanisms, Nan et al. [72] showed that at the same translational velocity, the roller outperforms the blade spreader in terms of the total particle volume of the spread layer only at a small ratio of the

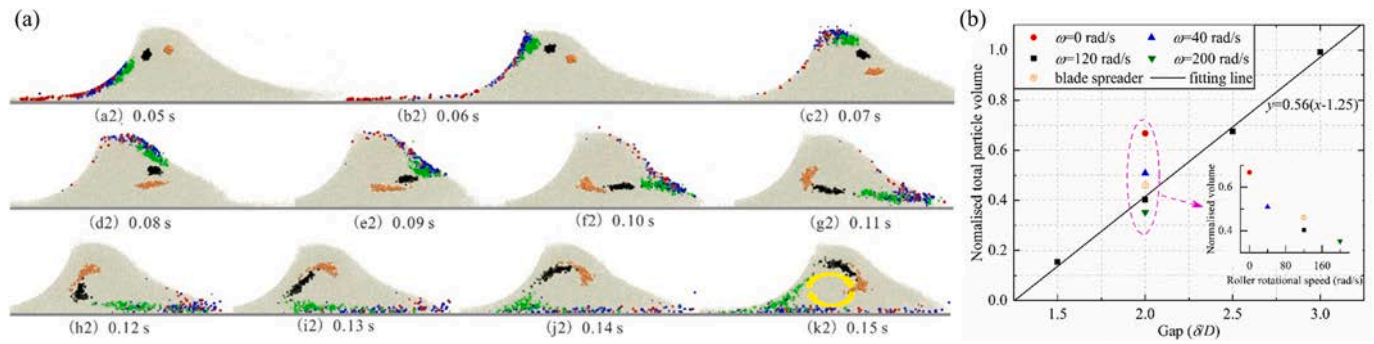

Fig. 8. Roller spreading system: a) particle convection and circulation within the heap, in which particles are lifted up by the roller and then cascade down on the heap slope before they are collected by the gap; b) variation of the total particle volume of the spread layer with the gap height, as reported by Nan et al. (2020).

rotational speed to translational speed, in which the critical ratio was around 1.0 in their work and 316 L stainless steel powder was used, as shown in Fig. 8. Cheng et al. [28] found that the packing density of the spread layer decreased monotonically with increase of the rotational speed. Similarly, Haeri et al. [36] analysed the layer quality based on the packing density and surface roughness for rod-like particles, and they found that roller spreading outperforms blade spreading under the same translation velocity of the spreader, as the roller geometry could provide a large contact area and allow for gradual particle rearrangement, while the blade, mainly interacted with the bed at a single point (its edge), dragging the particles as it moved which led to greater roughness of the spread layer. It should be noted that the ratio of the rotational speed of the roller to its translational speed in their work is constant, i.e. 1.0, which is close to the critical ratio as found by Nan et al. [72]. Oropeza et al. [33] experimentally found that the roller surface texture and roughness could not improve the layer density, but the hopper dispensing mechanism had a positive effect on the layer density. Zhang et al. [43] showed that larger roller diameter would exert more pressure on the powder compression zone and reduce the density of the spread layer.

Therefore, under the combined effects, such as convection and circulation of particles, dragging effect, dilation effect, particle arrangement, and particle segregation, which maybe inter-related, for most kinds of powder, roller spreading outperforms the blade spreading only at a small ratio of the rotational to translational speeds, at the same translational speed of the spreader. Of course, for very cohesive powder, the rotational movement of roller can break the agglomerates of particles in the heap and produce a denser layer, outperforming the blade spreading system. This was also followed by Wang et al. [74], in which they thought using a roller spreading system could greatly reduce the impact of particle cohesion on spreading performance. It is also observed in binder jet 3D printing technology of metal powder, but the effect of roller rotational movement (including speed and surface conditions) on the breaking of agglomerates of very cohesive powder has not been well understood till now.

For the effects of translational speed of roller on the spreading process, the mechanisms are similar to those of the blade spreading system. For example, Parteli et al. [38] found that with the increase of roller translational speed, the roughness of the spread layer increased, resulting in worse quality of spread layer. Chen et al. [57] investigated the relationship between the roller translational speed and the quality of the spread layer. They showed that the proportion of empty patches

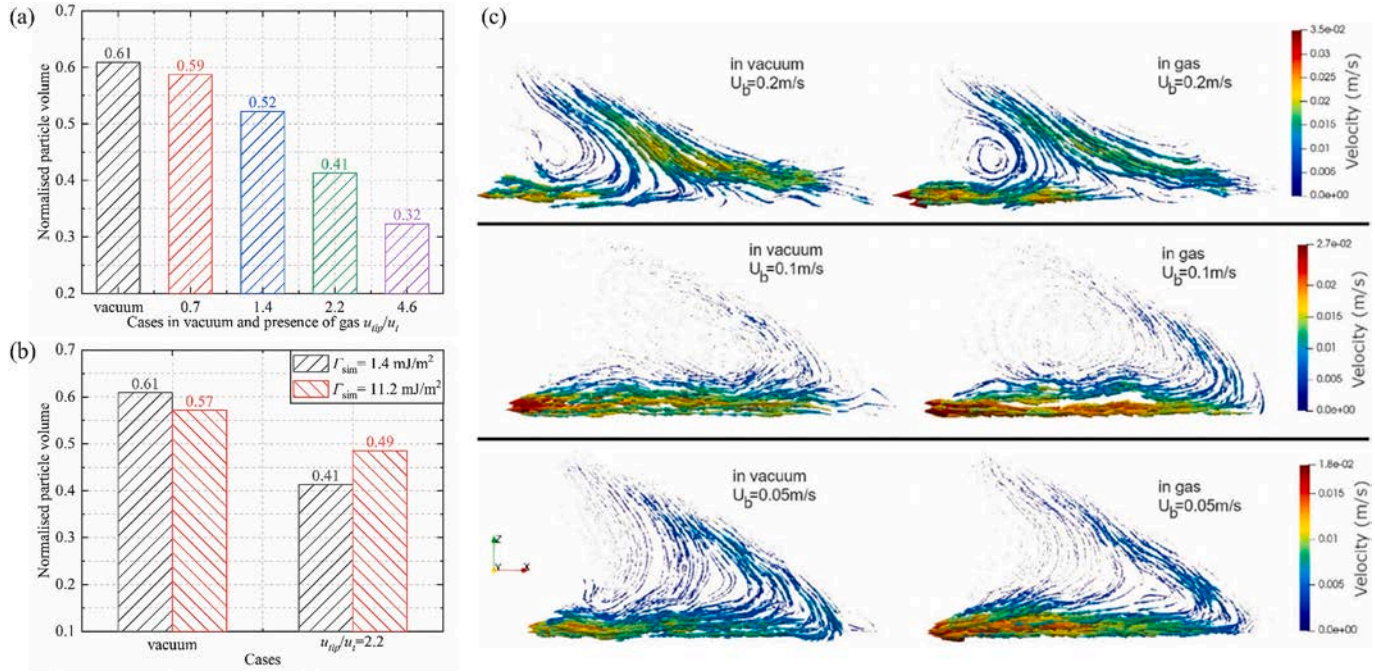

Fig. 9. Effect of the gas atmosphere on the spreading process: (a) and (b) total particle volume of the spread layer as reported in Nan et al. (2020), in which u_t is the terminal velocity of particle, u_{tip} is the tip speed of roller, and Γ_{sim} is the particle interfacial surface energy; (c) velocity vectors of particles as reported in Khajepor et al. (2023), in which U_b is the blade speed.

Table 3
Sensitivity parameters of fine metal powder to the presence of gas, as reported by Nan et al. (2024).

Parameters	Sandvik powder			Ancor powder			Formulations
	D_{10}	D_{50}	D_{90}	D_{10}	D_{50}	D_{90}	
Archimedes number	0.001	0.012	0.099	0.002	0.019	0.386	$Ar = \frac{\rho_f(\rho_p - \rho_f)gd^2}{\mu^2}$
Gas sensitivity index	0.88	0.73	0.60	0.83	0.70	0.51	$\xi = 1\text{-}ln\zeta/ln\zeta_c \text{with} \zeta = Ar\frac{\rho_p}{\rho_f}\zeta_c = 9.56 \times 10^6$
Terminal velocity (mm/s)	0.54	2.96	11.79	0.97	3.86	28.92	$u_t = \frac{\mu Re_t}{\rho_f d} \text{with} \frac{4}{3}\frac{Ar}{Re_t^2} = C_d(Re_t)^2$ $C_d = 24(1 + 0.15Re^{0.687})/Re$
Non-dimensional number (u_{tip}/u_t)	1392	256	64	783	196	26	–

* Ar is Archimedes number; ρ_f and ρ_p are the density of fluid and particle, respectively; g is gravitational acceleration; d is the particle diameter; μ is the dynamic viscosity of fluid; U_t and Re_t are the terminal velocity and corresponding Reynolds number, respectively; C_d and Re are the drag coefficient of particle and Reynold number, respectively.

increased with the increase of translational speed of the roller, due to the dragging effect as observed in the blade spreading system. Similar conclusion could also be found in Zhang et al. [43], Tan et al. [22] and Penny et al. [75]. For the effects of gap height on the roller spreading process, Tan et al. [22] had the same point as Nan et al. [76] that the narrow gap would cause more force arches and stronger jamming effect. Li et al. [77] experimentally analysed the effects of gap height on the quality of the spread layer based on CT image of the spread layer, and they showed that the spreading gap should be linked to the maximum particle size.

4.4. Effect of gas atmosphere

The gas atmosphere also has a significant effect on the spreading process. Nan et al. [76] considered the influence of inert gas (argon) on the roller spreading process by using the coupling simulation of discrete element method (DEM) and computational fluid dynamics (CFD), in which the dynamic mesh was adopted to account for the effect of roller action on fluid flow. They discovered that the presence of gas resulted in the deceleration of convection and particle circulation within the heap and a steeper heap repose angle. The quantity of particles spread on the work surface decreased compared to scenarios where gas drag was not taken into consideration. Interestingly, their results showed that particles with higher interparticle cohesion formed a more uniform spread layer with a greater total particle volume when gas drag was taken into account, indicating a coupling between the effect of the gas environment and particle cohesion, as shown in Fig. 9. They innovatively proposed a non-dimensional number to quantify the sensitivity of the spreading process to the gas environment, i.e. the ratio of the roller tip speed to the terminal velocity of an individual particle, in which a ratio much larger than 1.0 indicated that the spreading process was significantly sensitive to the gas environment. Khajepor et al. [78] simulated the influence of the gas environment on the blade spreading process of Inconel 718 powder using the coupling simulation of discrete element method for particles and lattice Boltzmann method for fluid, as shown in Fig. 9. They showed that the presence of inert gases increased the amount of deposited powder. As the blade speed increased, the disparity in powder deposition between the gaseous and vacuum surroundings became more pronounced. Moreover, it was observed that the newly deposited particles were disrupted by the wake of the blade, given that the gas velocity near the bed could exceed the terminal velocities of most particle size classes in the simulation. Recently, Nan et al. [48] calculated the gas sensitivity of 316 L stainless powder in binder jet 3D printing, as shown in Table 3. In this case, as the pressure in the printing chamber must be

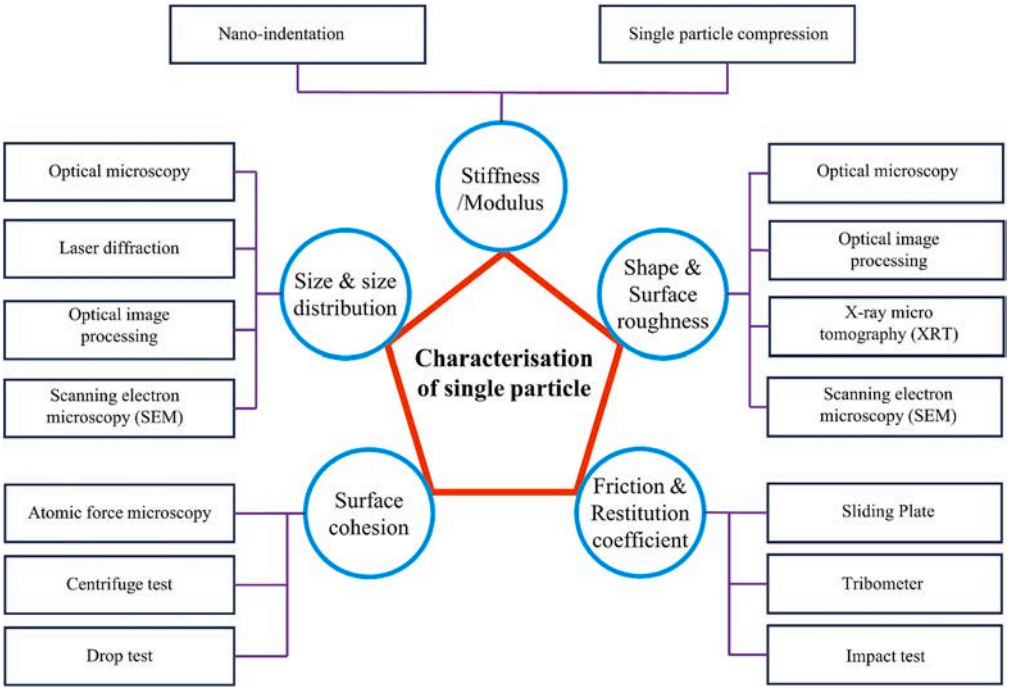

Fig. 10. Characterisation parameters and corresponding test methods for single particle.

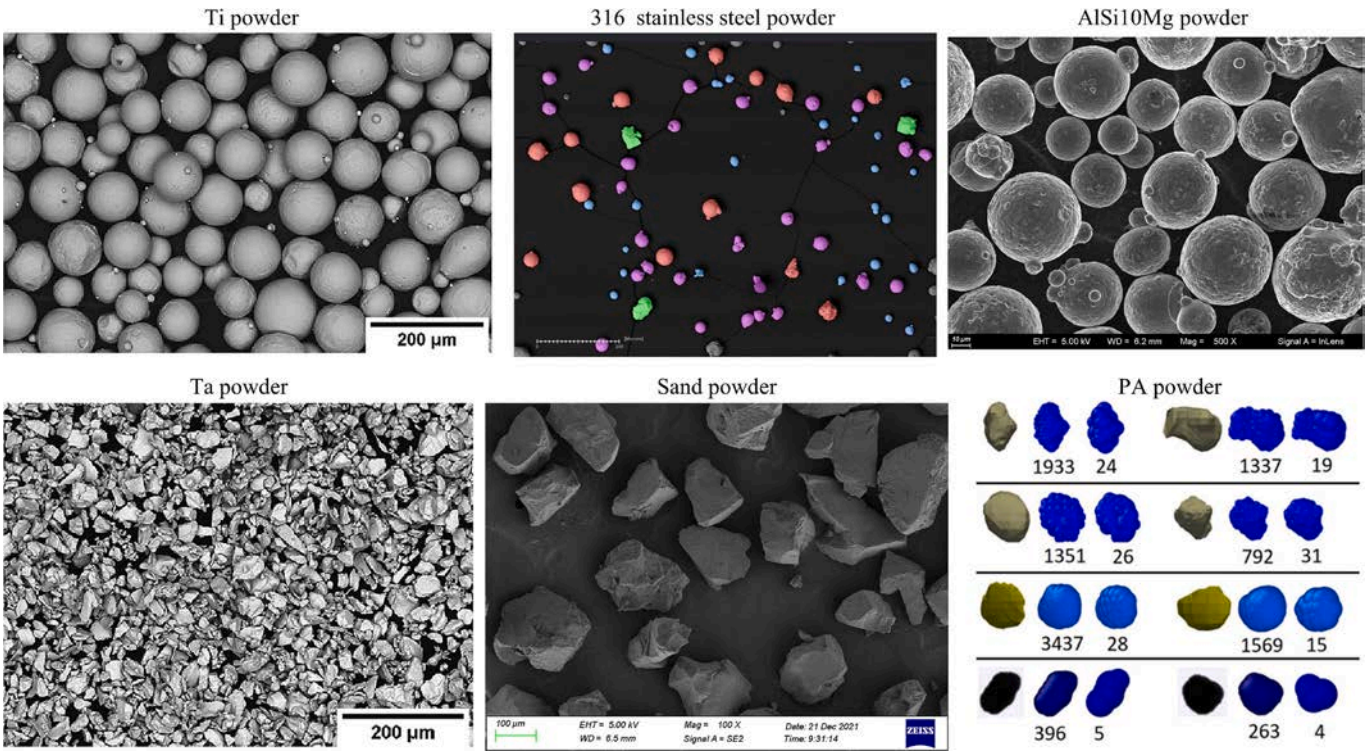

Fig. 11. The use of non-spherical particles in powder-based additive manufacturing: small and large clumps on the particle sphere as widely observed for metal powder using gas-atomised manufacturing methods, such as Ti powder, 316 L stainless steel powder, and AlSi10Mg alloy powder, as reported in Nan et al. (2018, 2022) and Silva et al. (2023); Ta powder manufactured at low cost, as reported in Silva et al. (2023); angular particles of sand powder as reported in Nan et al. (2024) and irregular particles of PA powder as reported in Nasato et al. (2020).

slightly higher than the internal pressure of the printhead to prevent the binder from dripping out, the spreading process occurs in a gas-filled environment instead of a vacuum. Applying the same analytical approach as that of Nan et al. [76], they demonstrated that both Sandvik and Ancor stainless steel powders were indeed responsive to the effects of the fluid medium and the gas flow induced by the roller action. Thus, it was intuitively expected that partial fluidisation of particles would be induced by the roller action, and the spreadability would be significantly affected by the presence of gas, especially for the Sandvik sample.

Based on above review, it is concluded that the spreading process is significantly affected by the gas environment when the ratio of the spreader speed to the terminal velocity is much larger than 1.0. It should be noted that although different kinds of gas may be used in different AM methods, for example, inert gas such as argon or nitrogen in SLM, air in binder jet 3D printing, their difference, i.e. viscosity and density, could be represented by the parameters and non-dimensional number shown in Table 3. However, there is still no further experimental work to validate these findings as the gas environment in a real AM machine is complex, including both the gas flow induced by the spreader action and the effect of gas flow in transporting the spatter away from the laser-scanned regions to the chamber outlet, especially in the SLM process.

5. Effects of particle properties

The particle properties, including particle size and shape, cohesion and surface roughness, differ greatly among different kinds of additive manufacturing methods. Characterisation and understanding of the various properties of powder at single particle scale play a crucial role in improving the quality of the spread layer in the manufacturing process. Many researchers have conducted abundant research on the effects of particle properties on the spreadability and spreading process. Fig. 10 summarises the parameters of the particle properties, which are of interest for powder spreading in AM. The corresponding characterisation methods are also included here. For example, surface cohesion (i.e. interfacial surface energy) could be measured by a drop test [79,80], in which the adhesion force is balanced by the detachment force during the impacting process, and particle shape could be re-constructed by the analysis of SEM images, as detailed described in Nan et al. [14]. Among these particle properties, the particle size and shape, as well as the particle cohesion, are of particular interest to researchers, and they are reviewed as follows.

5.1. Effect of particle shape

The introducing of irregular particles into the powder spreading process in additive manufacturing is usually due to two considerations: the shape of particles of the powder available is irregular, such as PA powder and sand powder; the powders with irregular particles are much less expensive than those with ideal spherical shapes, such as metal powder using a gas-atomised manufacturing method compared to the plasma rotating electrode-comminuting process (PREP). Examples of the shapes of particles of commercial powder are shown in Fig. 11, in which small and large clumps on the particle sphere are widely observed for metal powder using gas-atomised manufacturing methods.

The deviation of particle shape from sphere usually has a negative effect on the spreadability and spreading process, as observed in the experiments. Oropeza et al. [33] experimentally conducted a detailed study on the correlation between particle shape and layer quality via using a self-made experimental platform X-ray imaging technology. The degree of irregularly shaped particles was characterised via the median volumetric circularity, which was based on the perimeter and area of the projected particle image. They found that spherical particles had a better spreadability than irregular particles when the rotational motion of the spreader was imposed. They thought that it was due to the increased interparticle friction and poorer packing for the particles with irregular shapes. Recently, Nan et al. [81] conducted experiments on the

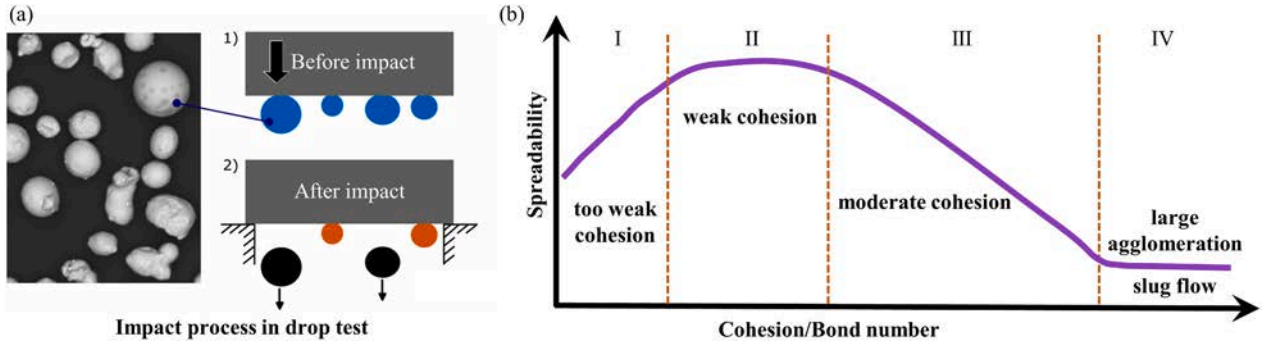

Fig. 12. Schematics of (a) drop test as reported by Pedrolli et al. (2024), in which the particles in blue are referred to the particle before impact, while the particles in orange and black are referred to the particles still adhered on the wall and detached after impact; (b) variation of spreadability with cohesion number or bond number. (For interpretation of the references to colour in this figure legend, the reader is referred to the web version of this article.)

spreadability of angular particles of sand powders. They found that the irregular shape of sand particles would produce more empty patches than spherical 316 L stainless steel powder at the same normalised gap height.

The effects of particle shape could also be represented by using a spherical shape but with a large rolling friction coefficient, to model the interlocking between particles. For example, Shaheen et al. [19] studied the effect of particle shape on the quality of the spread layer by changing the rolling friction coefficient. They found that for strongly cohesive particles, rolling friction coefficient had a significantly negative impact on the quality of the spread layer, on the contrary, sliding friction coefficient had an astonishing positive impact on the quality of the spread layer. Xu et al. [17] found that with the increase of rolling friction of particles, the interlocking between particles not only suspended the refilling process of particles within the heap, but also promoted particle jamming around the gap, resulting in a significant decrease of spreadability. They also demonstrated that as a result of particle jamming, powder spreadability was more sensitive to the rolling friction or particle interlocking than particle cohesion for the cases considered in their work.

However, for particles with a slender or rod-like shape, the non-spherical shape sometimes has positive effects on the spreadability and spreading process, as observed in DEM simulation, in which the particle shape is usually re-constructed by clumped spheres [36,38,65,81,82]. Haeri et al. [36] studied the spreading process of rod-shaped particles described by clumped spheres for blade and roller spreading systems. They explored the relationship between the particle shape and the quality of the spread layer characterised by the packing density and surface roughness. They found that the spread layer quality decreased with the increase of aspect ratio of rod-shaped particles. However, when the aspect ratio was 1.5, the counter roller would gain the best packing density. They attributed this to the more particle rearrangement and the more contact area between the particles and the roller. Similarly, Nasato et al. [65] conducted a study on the correlation between the particle shape and spreading quality of three kinds of commercial PA particles, in which the particle shape is described by using their developed multi-sphere reconstruction method, as shown in Fig. 11. They found that a larger aspect ratio of particles could increase the packing density of the spread layer. Compared to spherical particles, the quality of the spread layer was higher than that of the spherical particles, which was due to the higher probability of particle alignment when particles had thinner length and lower aspect ratio.

Silva et al. [32] experimentally evaluated the spreadability of a blend with spherical Ti and irregularly shaped Ta based on a double-toothed blade, to seek the potential of decreasing the material cost. They conducted standard flowability tests of a Ti—Ta blend and found that the flowability of the blend was between that of spherical Ti and irregularly shaped Ta powder. They also investigated the effects of the blade speed and gap height on the spread layer via SEM analysis, chemical analysis and micro-CT scanning. The corresponding results of their research demonstrated that it was feasible to use irregularly shaped particles to mix with spherical particles. Meanwhile, the DEM modelling of the spreadability of the mixture of powder and fibres is also attractive, which is usually used in selective laser sintering (SLS) to reinforce the polymer matrix and improve the mechanical properties of the components. Chen et al. [30,83] investigated the spreadability of mixtures of spherical particles and fibres with different lengths and diameters. They found that adding fibres with a diameter of 10 μm and a length of 15 μm could improve the spread layer density compared with that of spherical particles for both blade spreading and counter-rotating roller spreading. But longer fibres decreased the flowability of the powder mixture and reduced the spread layer density. Tan et al. [22] also investigated the effects of a mixture of spherical particles and fibres and found that when the weight fraction of the fibre was less than 10 %, the quality of the spread layer would be improved.

5.2. *Effect of particle cohesion*

Most of the particles used in additive manufacturing are relatively cohesive, so exploring the effects of particle cohesion on the quality of the spread layer could provide a good reference for the spreading process in actual production. Particle cohesion is referred to the extent of attractive interaction between two particles when they are separated from the state in contact. Based on the interfacial surface energy Γ, the cohesion of a single particle could be quantified by the bond number and cohesion number. The bond number (Bo) is the ratio of the maximum tensile force predicted by JKR theory [84] (i.e. a contact theory used to describe the contact mechanics between elastic bodies, accounting for both elastic deformation and adhesive force at the contact interface) to the particle weight (mg), and the cohesion number (Coh) is the ratio of the adhesive work to the gravitational potential energy of the particle with a characteristic height equal to the particle radius, given as [85,86]:

$$Bo = \frac{1.5\pi\Gamma R}{mg} \tag{6}$$

$$Coh = \frac{1}{\rho g}\left(\frac{\Gamma^5}{E^2R^8}\right)^{1/3} \tag{7}$$

where E is the Young's modulus, ρ is the material density, and R is the radius of the particle with a characteristic diameter of D_{90}.

It should be noted that although the interfacial surface energy of particle maybe roughly estimated from the Hamaker constant (a coefficient that relates the interactive van der Waals energy to the distance of separation between two molecules), the latter depends only on the solid material, while the interfacial surface energy is affected by both the solid material and the surface conditions of particle, especially the asperities

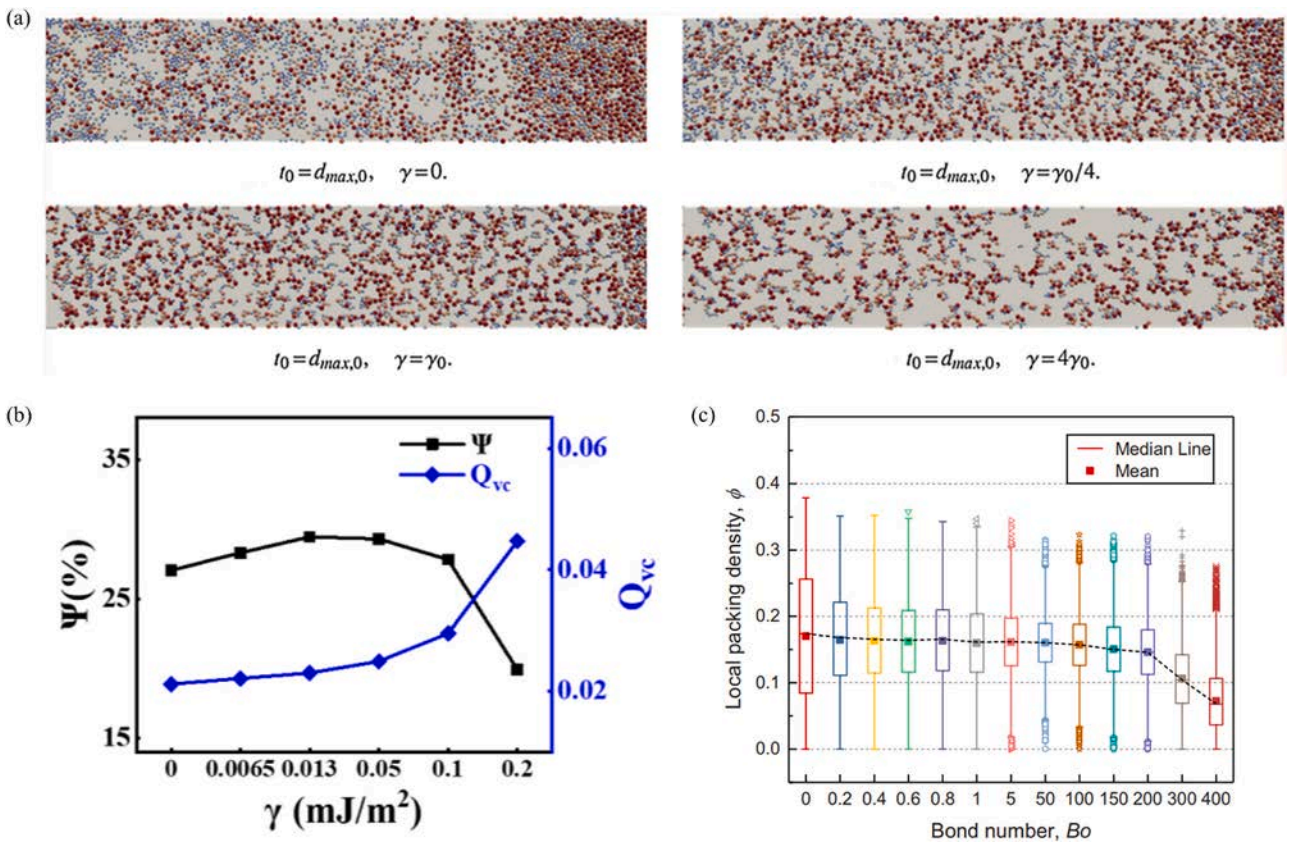

Fig. 13. Effects of particle cohesion on spreadability: (a) snapshots of the spread layer as reported by Meier et al. (2019), in which t_0 is the gap size, with the same meaning as δ, $d_{max,0}$ is the maximum particle size, γ is the particle surface energy, with the same meaning as Γ; (b) packing density and uniformity of the spread layer as reported by Si et al. (2021), in which ψ is the packing fraction, and γ is the particle surface energy, with the same meaning as Γ; (c) packing density of the spread layer as reported by He et al. (2020).

on the particle surface. For example, even for the same kind of powder material, i.e. gas-atomised 316 L stainless steel powder used in binder jet 3D printing technology, as measured by Nan et al. [48], the interfacial surface energy of a single particle can be 4.98 mJ/m^2, 9.68 mJ/m^2, depending on the powder supplier. However, the commercial tester for quick characterisation of the interfacial surface energy of particles at low cost is almost not available, resulting in that only a few of researchers measured the cohesion of single particle, such as the work of Nan et al. [14,48] using the in-house rigs of drop test [79,80], which is schematically illustrated in Fig. 12. On the other hand, most researchers usually characterised the flowability of bulk powder in the experiment and used it to quantify particle cohesion, for which several commercial methods and testers are available, as summarised in Table 1. It should be noted that bulk cohesion and flowability are affected not only by the cohesion of a single particle, but also by the shape and friction of the particles. The interfacial surface energy of single particle could also be roughly calibrated by using DEM simulation, in which the interfacial surface energy of single particle input in DEM simulation is adjusted to obtain similar flowability and bulk cohesion as the experiment. The angle of repose (AOR) of particle heap is mostly used [19,27,87], which is also the most simple and easiest experiment to be carried out. For example, Shaheen et al. [19] simulated the angle of repose and compared the results to experimental data of Ti-6Al-4 *V* powder, in which Young's modulus was scaled down to speed up the simulation.

Effects of particle cohesion as quantified by Coh/Bo number on the spreading process and spreadability are complex, which is schematically shown in Fig. 12. Too weak cohesion would make the powder too free flowing, and the particles are not easily to be deposited onto the rough work surface, as validated by the experiment of Nan et al. [72]. If the particle cohesion is too large, agglomeration would be formed, and then the spreading process is dominated by the jamming of agglomerates, even slug (full slip) flow, resulting in almost no particles spread onto the rough work surface. For particles with weak cohesion as quantified by Coh/Bo number, the spreadability does not show much variation when the particle cohesion is slightly increased. For particles with moderate cohesion, the increase of particle cohesion could slow down the detachment of particles from the heap into the gap, and the movement of particles within the heap, including the re-filling rate of the depletion region by gravity, resulting in the decrease of spreadability.

Above viewpoints have been clarified by various researchers [26,27,62,63,66,67,74,88,89]. Meier et al. [62] investigated the effect of particle cohesion on the packing density and surface roughness of spread layer, as shown in Fig. 13. They found that the high cohesion (small particle size) would reduce the quality of the spread layer, due to obstructing particle deposition driven by gravity. He et al. [88,89] conducted a detailed study on the impact of particle cohesion on the spreading process using DEM simulation, as illustrated in Fig. 13. Their findings demonstrated that increasing particle cohesion first decreased and then increased the cluster size. Additionally, it caused these clusters to align more perpendicular to the spreading direction. The median of local packing density remained relatively constant across a wide range of Bo values. An optimum level of particle cohesion was identified around Bo = 50, which exhibited minimal variations in local packing density, surface roughness, and pore sizes. Their findings also clarified that a better layer quality could be obtained either by small particles with weak surface cohesiveness or large particles with moderate surface cohesiveness. Moreover, reducing particle size could enhance density uniformity for lightly cohesive particles but not for significantly cohesive particles. They considered that the layer quality was controlled by two competing effects: the geometrical effect arising from the constraint

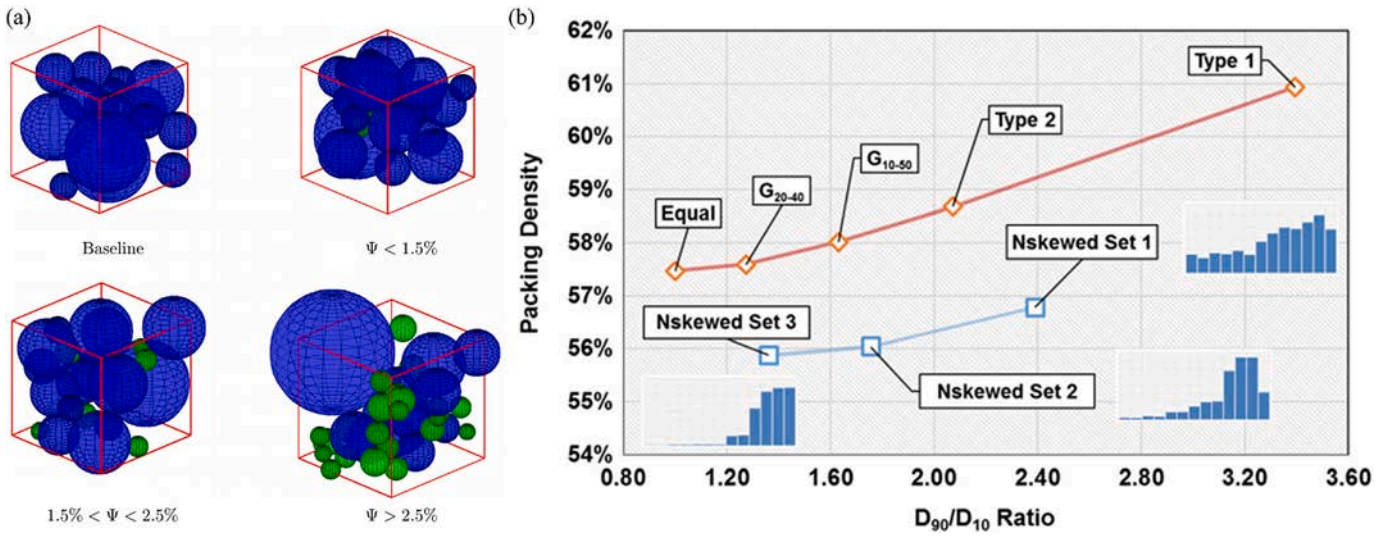

Fig. 14. Effect of particle size distribution on spreadability: (a) three-dimensional representation of micro-structure with different fraction as reported by *Ma* et al. (2020); (b) Packing density with different D_{90}/D_{10} ratios as reported by Lee et al. (2018),

of gap height and the cohesive effect as characterised by bond number, and the cohesive effect took over geometrical effect as the dominant factor governing particle spreading process when Bo >100. Their work was further followed by Wu et al. [63] and Si et al. [27]. Si et al. [27] found that with the increase of particle cohesion, the quality of the spread layer would first increase, and then decrease, as shown in Fig. 13, in which they thought larger particle cohesion could lead to the decrease of flowability and induce the particle agglomerations of fine particles. Wu et al. [63] thought that the cohesion of particles would be reduced by increasing the particle size, resulting in effective improvement of the packing density of the spread layer, but the surface roughness became worse due to the wall effects of large particles. They also thought that the gravity-induced particle deposition might be hindered by the formation of force arches when the cohesion between particles increased. It should be noted that the powder is spread onto the recently melted or heated layer, which is usually at high temperature, especially in SLM system. This high temperature would impose significant effects on the particle properties, especially the interfacial surface energy, as clarified by Ruggi et al. [53], in which shear cell tests were carried out for nylon powders at different temperatures. If assuming the temperature of the particles within the powder heap is constant everywhere, i.e. all particles have the same interfacial surface energy, the effect of temperature on the spreading process could be inferred from previous work focussing on the effect of particle cohesion. This method was adopted by Ajabshir et al. [90] to model the effect of temperature on the spreading process. However, in reality, the temperature varies within the powder heap through conduction, i.e. particles close to the base have a higher interfacial surface energy due to a higher temperature than the ones remote from the base, which makes the effect of temperature on the spreading process much more complex.

5.3. *Effect of particle size and size distribution*

Particle size range is usually determined by the specified additive manufacturing method. The particle size is usually around 15–53 μm for selected laser melting (SLM) [14,39,47,91] and 45–106 μm for electron beam melting (EBM) [32,64]. For example, in SLM, D_{50} = 32 μm and D_{90} = 45 μm for 316 L stainless steel powder [14], and D_{90} = 46 μm for Ti6Al4V powder [6]. For the binder jet 3D printing process, it is usually less than 15 μm for metal powder [48,52], such as D_{90} = 7.5 μm for gas-atomised 316 L stainless steel powder [48], while it is usually in a much larger size (i.e. 140–250 μm) for sand 3D printing [81,92,93], such as D_{90} = 207 μm [81]. Finer particles would produce stronger cohesion, and they are more prone to induce poor packing density and surface roughness of the spread layer [33,38,94,95]. Meanwhile, Finer particles also demonstrate more requirements on the spread conditions. For example, in binder jet 3D printing of metal powder, due to the restriction of binder-particle interactions, the particle size is usually very fine, and in this case, the roller spreader with a large tip speed (to break the agglomerates) is usually required, as reported by Nan et al. [48].

On the other hand, without much change in the particle size, the size distribution could be optimised for different materials, which is more attractive and practical in reality. Several researchers [6,39,62,74,96–99] have found that the percentage of small particles within the size distribution played an important role. For example, Lee et al. [97] simulated the effects of four types of PSD on the packing density, including negatively skewed, equal-sized, Gaussian, and positively skewed PSD. Their results showed that a high proportion of small particles would improve the layer quality for the same type of PSD, while the mean radius had a negligible effect on the packing density, but the dependence of the packing density on the type of PSD was relatively weak, as shown in Fig. 14. Meier et al. [62] also observed similar results, but their simulation results claimed that too large proportion of very fine particles would decrease layer quality. Wang et al. [74] found that the wider range of particle size had better spreadability than the narrow one in two kinds of spreading systems based on DEM simulation, due to a larger number of small particles filling the space between coarse particles. *Ma* et al. [96] found that adding a small number of fine particles to the baseline material could slightly improve the quality of spread layer, as the fine particles would fill the space between particles, which is detailed illustrated in Fig. 14. Recently, Salehi et al. [98] carried out experimental research on the effects of the particle size distribution of 12 kinds of powders. They found that the powders with a narrow particle size distribution had higher relative packing fractions than the powders with a wider particle size distribution. On the other hand, the existence of too large particles may cause problems for powder spreading process due to the jamming effect [14], which may lead to significant defects within the spread layer, such as uneven distribution of particles and empty patches, as reported by Cordova et al. [29], Shaheen et al. [19] and Zhang et al. [99]. Therefore, by adjusting the PSD of powder while avoiding the powder from being polluted by excessively large particles, the quality of the spread layer could be improved to some extent. However, it should be noted that the addition of fine particles or increasing the proportion of fine particles within the PSD should not significantly change the spreading behaviour or flowability of the original materials too much, otherwise, the spreadability would be

Table 4
Summary of the defects of the spread layer need to be monitored during the spreading process.

Defects	Description
Spreading dynamics related to defects	***Protruding part:*** locally overheated regions of fused part would curl upwards; if this deformation exceeds the layer thickness, the spreader collides with the protruding part. ***Mechanical jamming:*** particles are transiently and intermittently jammed due to relatively narrow constriction between the spreader and fused part, resulting strong force chain. ***Cohesive jamming or slug:*** strong particle agglomerates exist in the powder heap, and they are jammed in front of the constriction.
Large-scale defects (Incomplete spreading)	Not enough amount of powder within the heap to cover the whole work surface of fused part due to *overdose factor or shielding gas flow reduction.* Not enough powder to be allowed to pass through the gap due to *protruding part* or *cohesive jamming/slip* although the amount of powder within the heap is sufficient.
Medium-scale defects	***Ripples:*** during the impacting/striking against protruding part, the spreader is first tensed and then released, resulting in a bouncing/recoiling behaviour, followed by formation of ripples. *Feature*: a long line-styled empty patch perpendicular to spreading direction (also called hopping). ***Grooves:*** discrete spatters (due to sintering defects) on the fused part, which are usually in large size, or relatively large particles within the bulk powder, are dragged across the spread layer by the spreader, resulting in grooves. *Feature*: a long line-styled empty patch parallel to spreading direction (also called streaking). ***Ridges:*** if the spreader is damaged at any point due to strong force generated during *protruding part or jamming*, ridges may occur in subsequent layers. *Feature*: a long line-styled empty patch parallel to the spreading direction (also called streaking).
Small-scale defects	***Discrete empty patches:*** if transiently and intermittently mechanical jamming is involved due to unproperly settled layer thickness or large roughness of fused part due to sintering defects (such as *balling*), discrete empty patches with small size and irregular shapes would be formed. ***Scattered particles:*** ejection of particles into the spread layer due to sudden bouncing/recoiling of spreader against the protruding part, or the quick collapse of mechanical jamming, resulting in large roughness of the spread layer. ***Discrete agglomerations:*** some particles within the spread layer are adhered to each other, resulting in large roughness of the spread layer.

reduced.

6. Defects and optimisation

6.1. Defects and detection

During the powder spreading process in additive manufacturing, defects within the spread layer have always been an issue that cannot be ignored, as they would cause problems with the quality of the final product, and even make the manufacturing process stop. The defects could be classified into two types: 1) the work surface is fully covered by particles, but the spread layer is not good, in terms of large roughness (i.e. particle agglomeration) or low packing density at local regions; 2) there are empty patches within the spread layer, i.e. the work surface is not fully covered by particles, with sizes ranging from a few of particle diameter to several millimetres or even centimetres. A summary of the description of the defects and related spreading dynamics is listed in Table 4, where only the defects that occurred in the spreading process are included. One main cause of the defects is particle jamming, especially for the formation of empty patches. When the particles pass through the narrow gap between the spreader and rough work surface, they may be jammed within or in front of the gap. As summarised by Nan et al. [81], particle jamming in the spreading process could be classified into mechanical jamming, cohesion-induced jamming, combined jamming, and slug flow, as shown in Fig. 15(a).

The primary adverse effect of particle jamming on the formation of the spread layer is the transient halt of particle flow, leading to an inadequate outflow of particles from the gap during the survival period of particle jamming. It should be noted that if the powder is highly cohesive, leading to the formation of strong particle agglomerates within the heap, particle jamming could be significant, even resulting in the occurrence of slug (full slip) flow of particles. The large empty patches in the experiments of Nan et al. [81], and the simulations of Meier et al. [62] and Xu et al. [17] are mainly due to this kind of jamming (i.e. cohesive jamming or slug), as shown in Fig. 15(b). For most kinds of powder used in AM machines, mechanical jamming and combined jamming (i.e. the jamming is caused by a combination of mechanical and cohesion-induced effects) are more likely to occur due to various factors. The empty patches observed in the work of Shaheen et al. [19] are actually caused by this kind of particle jamming: large particles are jammed, and then the jammed particles and their neighbours in contact with them are pushed and dragged forward by the spreader, preventing other particles from flowing through the gap and resulting in a long scratch of empty patches. Their simulation results agree well with the experimental results shown in Nan et al. [81], Yadav et al. [100], Cordova et al. [29], and Scime et al. [101], where some stripes named as grooves are observed in the spread layer due to the existence of very large particles (i.e. particle size distributions are not well controlled before use) or particles with extremely high friction, or agglomerates, as shown in Fig. 15(c).

Besides the halting of particle flow, Nan et al. [14] found that the mechanical jamming also has another adverse effect on the spread layer: a strong contact force network is developed and a large amount of large strain energy is stored during the survival period of jamming, as further verified by their experiments, where the force exerted on the baseplate by particles exhibits notably large peaks during the spreading process; this energy would release suddenly and kick away the jammed particles from the gap once the jamming state is broken by the moving spreader, resulting in a significantly non-uniform distribution of particles and particle segregation within the spread layer. Under these effects, when the local gap is narrow, empty patches could also be induced even if there are no very large matter, but the size of empty patches is much smaller than the ones shown in Fig. 15(c). This kind of defect has been widely observed in various studies, such as the simulation of Marchais et al. [26] and Nan et al. [14], and the experiments of Ahmed et al. [16]. Meanwhile, under the effect of the sudden release of a large amount of strain energy when mechanical jamming is collapsed, some particles may fly into the sky with position much higher than the gap. This process was also called particle bursting in Nan et al. [14] and particle ejection in Ajabshir et al. [90], which would cause scattered particles on the well-formed spread layer, as observed in Fischer et al. [102]. It should be noted that the jamming could also cause the wear of the spreader, especially when protruding part occurs, would change the surface conditions of the spreader, as reported by Ge et al. [103], which may affect the contact between the spreader and the particle or heap, resulting in problems related to the consistency of the spreading process and layer quality.

Many defects in manufacturing processes can be rectified in real-time by repeating the spreading jobs or adjusting the amount of powder delivered or the spreading conditions, including the gap height or layer thickness, and the speed of spreader. For instance, ridge-type defects can be mitigated by replacing the spreader between build jobs. Therefore, the detection of defects is crucial to determine whether such adjustments are necessary. Most detection methods rely on the analysis of the image

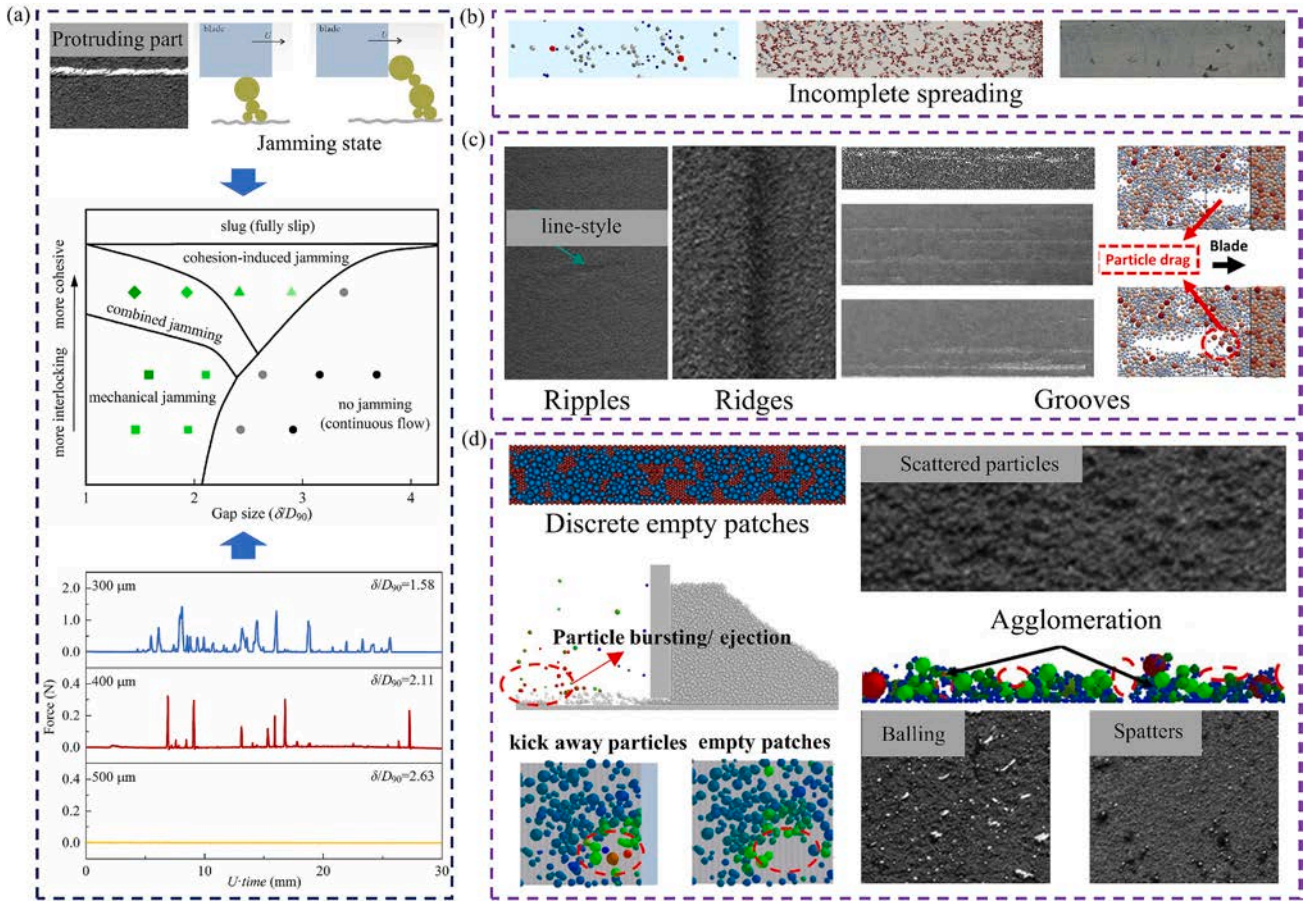

Fig. 15. Defects within the spread layer: (a) spreading dynamics related to defects: protruding part as reviewed by Fischer et al. (2022), particle jamming map and evidence as reported by the experiment of Nan et al. (2023); (b) large-scale empty patches due to cohesion-induced jamming or slug (full slip) in the experiment of Nan et al. (2023) as well as simulation of Xu et al. (2023) and Meier et al. (2019); (c) medium-scale defects: ripples and ridges as reviewed by Fischer et al. (2022), grooves observed in the experiment of Nan et al. (2023) and Cordova et al. (2020) as well as simulation of Shaheen et al. (2021); (d) small-scale defects: discrete small empty patches in the simulation of Marchais et al. (2021), particle bursting/ejection as well as kicking phenomenon due to the collapse of mechanical jamming in the simulation of Nan et al. (2018), scattered particles and balling as well as spatters reported in the experiment of Fischer et al. (2022), agglomeration of particles within the spread layer as observed in the simulation of Si et al. (2021).

of the spread layer. The detection of defects in DEM simulation could be easily realised through the snapshots of the spread layer, and an example was given in Desai et al. [104], where the roughness and porosity of the spread layer were calculated. However, in the experiment, due to various factors affecting the quality of the image of the spread layer, the detection is much more difficult than that used in DEM simulation, thus, the machine learning aided method is attractive and used by various researchers. Bartlett et al. [105] introduced a novel method incorporating in-situ three-dimensional digital image correlation (3D-DIC) to identify and quantify the severity of irregularities in the spread layer. Similarly, Ansari et al. [106] proposed a new approach to identify the defects of spread layer from in-situ layer images by employing a convolutional neural network (CNN) to obtain high-quality and high-resolution near-infrared (NIR) images. Yadav et al. [100] used CNN for monitoring the overall quality of builds, employing two CNN layers to process pre and post-exposure images. Additionally, they integrated in-situ melt pool monitoring (MPM) into the detection process. These advanced methods demonstrate the effectiveness of machine learning in defect detection in powder spreading process.

Recently, Scime et al. [101,107,108] successfully applied the multi-scale CNN algorithm to autonomously detect and classify spreading anomalies in real AM machines, as shown in Fig. 16(a). The input layer was modified to allow the algorithm to learn the appearance of layer anomalies and key contextual information across multiple size scales. These modifications to the CNN architecture were proven to enhance the algorithm's flexibility and overall classification accuracy while reducing human biases. They [101] further proposed a novel architecture named as dynamic segmentation CNN for pixel-wise localization (semantic segmentation) of layer-wise powder bed imaging data, which had the ability to return segmentation results at the native resolution of the imaging sensor and provide real-time performance. Across six different machines (including SLM, EBM and binder jetting), the validation true-positive and false-positive rates ranged from 99.8 %-15.7 % and 0.4 %–43.6 %, respectively, while the testing true-positive and false-positive rates ranged from 99.7 %–31.5 % and 1.1 %–57.0 %, respectively. Fischer et al. [102] established a comprehensive system for the detection of the inhomogeneities of spread layer in LPBF, as shown in Fig. 16(b), including the set-up of the rigs acquiring images using darkfield lighting, diffuse lighting and coaxial lighting, and the software/code for the training and detection of defects based on machine learning. In their work, images of more than 45,000 annotated anomalies of spread layer were acquired using a line camera with 6 μm/pixel resolution, and 99.15 % classification accuracy was achieved across seven classes using the Xception network architecture pre-trained on ImageNet.

6.2. *Optimisation methods*

The quality of the spread layer and spreadability could be optimised through several methods: the choice on the powder materials (such as shape, size and cohesion) and the usage of roller or blade as a spreader

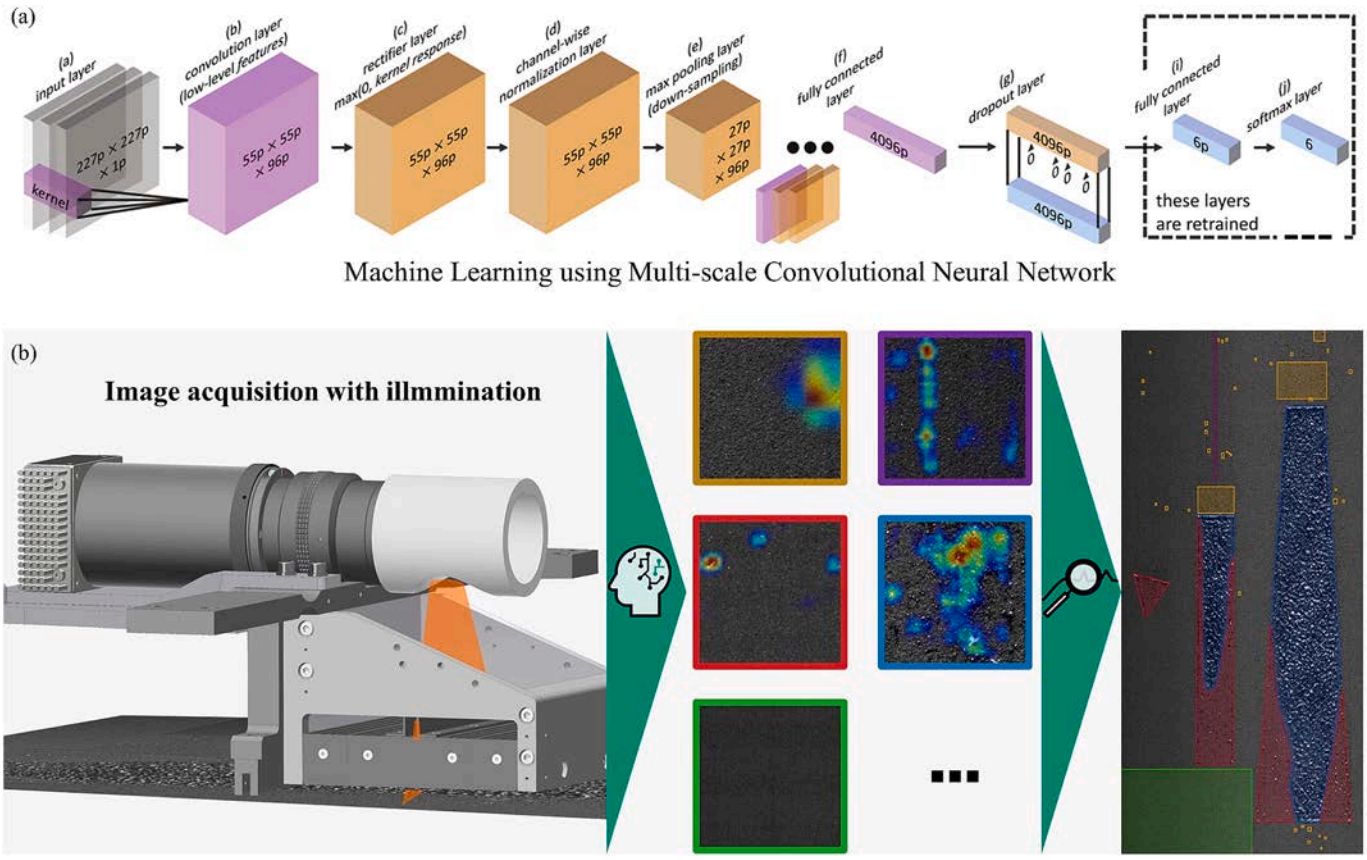

Fig. 16. Application of machine learning for the detection of defects within the spread layer: (a) Flowchart of the implementation of the multi-scale CNN technique as reported by Scime et al. (2018); (b) in-situ system proposed by Fischer et al. (2022).

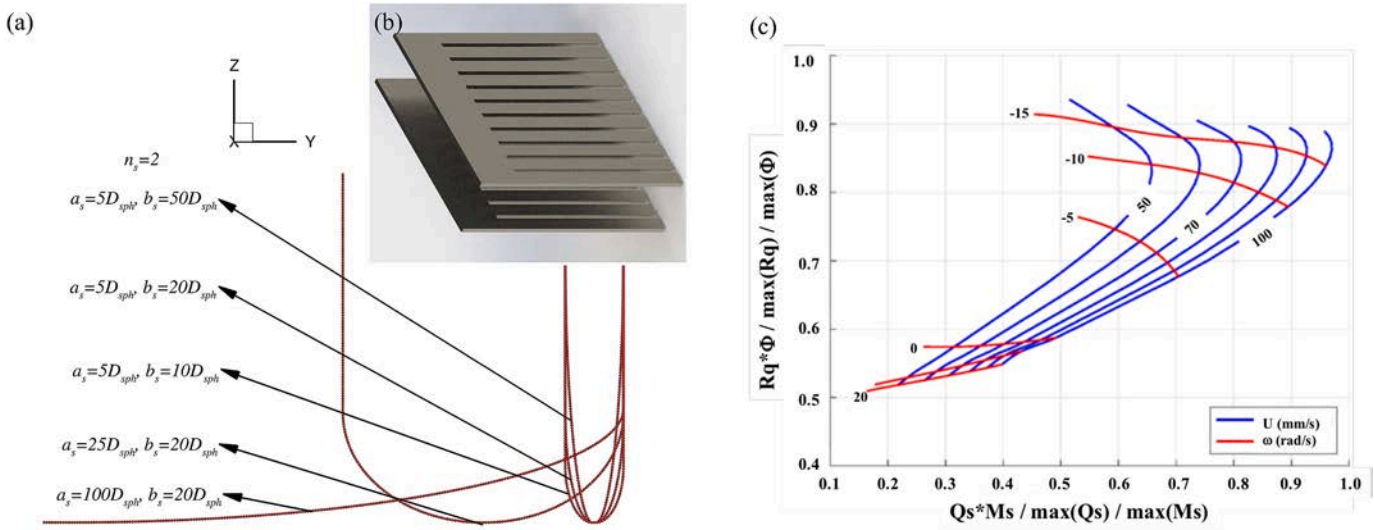

Fig. 17. Optimisation of the spreader and spreading conditions: (a) spreader profile as reported by Haeri et al. (2017), in which n_s, a_s and b_s are the parameters used to control the overall shape, width and height of the blade profile, respectively; (b) double-toothed blade as reported by Phua et al. (2021); (c) spreading process map as reported by Desai et al. (2019), in which M_s is the total mass of particles in the sampling region, Q_s is the volume of powder spread per unit time per unit width of spreader, R_q and Φ are the surface roughness and particle fraction of the spread layer, respectively, U and ω are the translational speed and rotational speed, respectively.

before the in-reality production process, in-situ optimisation of the spreading conditions (gap height or layer thickness, and speed of spreader) based on defect detection, the introduction of spreader vibration and the optimisation of the geometry shape of spreader. The first one could be carried out based on the understanding of the spreading mechanisms as well as the database generated in experiments and simulations, which has been studied by many researchers and reviewed above. The second one could be realised by using machine learning aided techniques, such as convolutional neural network (CNN), back propagation neural network (BPNN). For example, a process map with

hybrid parameters of translational speed and rotational speed of the roller was plotted by Desai et al. [104], as shown in Fig. 17, which could be installed in a 3D printer to provide a layer-wise control of defects as a function of spreader speed. Wu et al. [109] used a back propagation neural network (BPNN) model to predict and evaluate the layer quality, in which 25 sets of data obtained from DEM simulation were used, and a process map was also developed.

The spreading performance of very cohesive powder could be improved by applying vibration to the spreader. The vibration of the spreader can effectively destroy the agglomeration and separate them onto the work surface, as well as adjusting the arch structure of the force chain around the spreader. However, limited work has been done on the choice of vibration parameters, such as frequency and amplitude. Nasato et al. [82] investigated the role of vibration on the spreadability and spreading process of PA12 particles, in which the particle size D_{90} was about 82 μm. They concluded that the vibration only improved the packing density of the spread layer when the frequency and amplitude of the vibration were well chosen in combination with the specified translational speed of the blade spreader. However, the gap height in their work is very large, and the effects of vibration on other kinds of spreading conditions with narrower gap height and also other kinds of powder materials are still unclear, especially for the extremely cohesive powder in binder jetting 3D printing of metal powder. Meanwhile, the corresponding experimental data of the effects of spreader vibration on powder spreading process is also rare.

The spreader is an indispensable and important part of the spreading process, and its shape and geometry size are of great concern for the optimisation of spreadability and layer quality. Haeri et al. [110] proposed a new blade with a modified head profile, i.e. a supper-ellipse with three adjustable parameters, as shown in Fig. 17. By adjusting the three parameters of supper-ellipse, the overall shape, width and height of the blade could be defined. A set of 48 device-scale DEM simulations were performed and the optimum values for these parameters were identified in their research. They concluded that the optimised blade could generate a larger packing fraction of the spread layer than that of the traditional blade. Recently, Phua et al. [111] proposed a composite blade, in which two toothed blades were offset 2.5 mm apart and staggered, i.e. the aperture in the leading blade aligned with the centre of the trailing blade teeth, as shown in Fig. 17. Their simulation results demonstrated that this new kind of blade could filter large particles to flow through the teeth while forcing fine particles to flow underneath the blade. In addition to adjusting the overall geometric shape of the blade, the blade could also be optimised by only slightly modifying its bottom edge [66,98,112]. For example, Wu et al. [112] designed a half-arc blade, which combined the features of a straight shape from the vertical blade and an arc shape from the arc blade.

7. Future work

The effects of particle properties and spreading conditions on spreadability and spreading conditions have been extensively explored, but there are still some issues needed to be addressed in the future. In particular, the spreading of very fine powders, such as those less than 15 μm or even approximately 1 μm, in which strong agglomerates may be formed, need to be explored in detail, including the optimisation of vibration conditions and geometry of the spreader. Moreover, the use of low-cost powders is attractive for manufacturers, especially for metals with very high melting point, such as Ta powder; however, the particle shape of these kinds of powders is usually not spherical. Thus, exploring the effect of the particle shape on the spreading process or the feasibility of the mixture of powder with irregular and spherical particle shapes also needs to be addressed in the future. On the other hand, there is a complex relationship between AM part quality and powder spreadability, which also deserves in-depth study in the future.

With the aid of artificial intelligence (AI) or machine learning, in-situ detection of defects within the spread layer, and auto-adjustment of the spreading conditions to minimise the effects of defects on subsequent manufacturing processes, are attractive for commercial AM machines. Several articles have proposed wonderful detection algorithms as well as image acquisition systems, but the efficiency in terms of time is still doubtful for large-scale fused parts, which is critical for auto-adjusting the spreading conditions. The combination of image-based and force-based detection methods maybe more suitable for addressing diverse defects. For the latter, a force sensor could be assembled with the spreader to quickly monitor the occurrence of particle jamming. Moreover, machine learning based algorithms of subsequent adjustment of the spreading conditions based on the results of defect detection have not been well explored till now, but it is important and attractive for commercial AM machines to achieve intelligent manufacturing.

CRediT authorship contribution statement

Wenguang Nan: Writing – review & editing, Writing – original draft, Visualization, Supervision, Investigation, Funding acquisition, Formal analysis, Data curation. **Lanzhou Ge:** Writing – original draft, Visualization, Investigation, Formal analysis, Data curation. **Ziming He:** Writing – review & editing. **Zhonggang Sun:** Funding acquisition. **Jinzhong Lu:** Funding acquisition.

Declaration of competing interest

The authors declare that they have no known competing financial interests or personal relationships that could have appeared to influence the work reported in this paper.

Data availability

Data will be made available on request.

Acknowledgments

The authors are grateful to the National Key Research and Development Program of China (Grant No. 2023YFB4606000) and the National Natural Science Foundation of China (Grant No. 51806099). The first author is thankful to Professor Mojtaba Ghadiri, University of Leeds, UK, for his inspiration on this work, and the support and discussions on previous work on powder spreading from Drs. Mehrdad Pasha, Tina Bonakdar, Alejandro Lopez, Umair Zafar, Sadegh Nadimi, Wei Pin Goh, University of Leeds, UK.

References

[1] S.M. Thompson, L. Bian, N. Shamsaei, A. Yadollahia, An overview of direct laser deposition for additive manufacturing; Part I: Transport phenomena, modeling and diagnostics, Addit. Manufact. 36 (2015) 62.
[2] S.F. Shirazi, S. Gharehkhani, M. Mehrali, H. Yarmand, H.S. Metselaar, N. Adib Kadri, N.A. Osman, A review on powder-based additive manufacturing for tissue engineering: selective laser sintering and inkjet 3D printing, Sci Technol, Adv. Mater. 16 (2015) 033502.
[3] D. Yao, X. An, H. Fu, H. Zhang, X. Yang, Q. Zou, K. Dong, Dynamic investigation on the powder spreading during selective laser melting additive manufacturing, Addit. Manuf. 37 (2021).
[4] C. Körner, Additive manufacturing of metallic components by selective electron beam melting-a review, Int. Mater. Rev. 61 (5) (2016) 361–377.
[5] J.L. Bartlett, X. Li, An overview of residual stresses in metal powder bed fusion, Addit. Manuf. 27 (2019) 131–149.
[6] T.M. Wischeropp, Claus Emmelmanna, Milan Brandtb, A. Paterasb, Measurement of actual powder layer height and packing density in a single layer in selective laser melting, Addit. Manufact. 28 (2019) 176–183.
[7] A. Aramian, N. Razavi, Z. Sadeghian, F. Berto, A review of additive manufacturing of cermets, Addit. Manuf. 33 (2020).
[8] M.A. Balbaa, A. Ghasemi, E. Fereiduni, M.A. Elbestawi, S.D. Jadhav, J.P. Kruth, Role of powder particle size on laser powder bed fusion processability of AlSi10mg alloy, Addit. Manuf. 37 (2021).
[9] A. Mostafaei, C. Zhao, Y. He, S. Reza Ghiaasiaan, B. Shi, S. Shao, N. Shamsaei, Z. Wu, N. Kouraytem, T. Sun, J. Pauza, J.V. Gordon, B. Webler, N.D. Parab, M. Asherloo, Q. Guo, L. Chen, A.D. Rollett, Defects and anomalies in powder bed

fusion metal additive manufacturing, Curr. Opinion Solid State Mater. Sci. 26 (2022).
[10] M.H. Sehhat, A. Mahdianikhotbesara, Powder spreading in laser-powder bed fusion process, Granul. Matter 23 (2021).
[11] L.C. Capozzi, A. Sivo, E. Bassini, Powder spreading and spreadability in the additive manufacturing of metallic materials: a critical review, J. Mater. Process. Technol. 308 (2022).
[12] G. Miao, W. Du, Z. Pei, C. Ma, A literature review on powder spreading in additive manufacturing, Addit. Manuf. 58 (2022).
[13] Additive Manufacturing—General Principles—Fundamentals and Vocabulary, ISO/ASTM 52900, 2021.
[14] W. Nan, M. Pasha, B. Tina, L. Alejandro, Z. Umair, N. Sadegh, M. Ghadiri, Jamming during particle spreading in additive manufacturing, Powder Technol. 338 (2018) 253–262.
[15] M. Ghadiri, M. Pasha, W. Nan, C. Hare, V. Vivacqua, U. Zafar, S. Nezamabadi, A. Lopez, M. Pasha, S. Nadimi, Cohesive powder flow: trends and challenges in characterisation and analysis, Kona Powder Part. J. 37 (2020) 3–18.
[16] M. Ahmed, M. Pasha, W. Nan, M. Ghadiri, A simple method for assessing powder spreadability for additive manufacturing, Powder Technol. 367 (2020) 671–679.
[17] R. Xu, W. Nan, Analysis of the metrics and mechanism of powder spreadability in powder-based additive manufacturing, Addit. Manuf. 71 (2023).
[18] M. Hiroaki, K. Higashitani, H. Yoshida (Eds.), Powder Technology Handbook, Third edition, CRC Press, New York, 2006.
[19] M.Y. Shaheen, A.R. Thornton, S. Luding, T. Weinhart, The influence of material and process parameters on powder spreading in additive manufacturing, Powder Technol. 383 (2021) 564–583.
[20] H. Chen, T. Cheng, Z. Li, Q. Wei, W. Yan, Is high-speed powder spreading really unfavourable for the part quality of laser powder bed fusion additive manufacturing? Acta Mater. 231 (2022).
[21] Q. Han, H. Gu, R. Setchi, Discrete element simulation of powder layer thickness in laser additive manufacturing, Powder Technol. 352 (2019) 91–102.
[22] P. Tan, F. Shen, W.S. Tey, K. Zhou, A numerical study on the packing quality of fibre/polymer composite powder for powder bed fusion additive manufacturing, Virtual Phys. Prototyp. 16 (2021) S1–S18.
[23] R. Della Gatta, V. Lampitella, M. Trofa, G. D'Avino, D. Borrelli, A. Caraviello, A. Astarita, Reducing the energy density in selective laser melting of an Al-Si-Mg-Cu alloy through an improved spreading process of the powder bed, CIRP J. Manuf. Sci. Technol. 38 (2022) 813–823.
[24] S. Yim, H. Bian, K. Aoyagi, K. Yamanaka, A. Chiba, Effect of powder morphology on flowability and spreading behavior in powder bed fusion additive manufacturing process: a particle-scale modeling study, Addit. Manuf. 72 (2023).
[25] V. Lampitella, M. Trofa, A. Astarita, G. D'Avino, Discrete element method analysis of the spreading mechanism and its influence on powder bed characteristics in additive manufacturing, Micromachines (Basel) 12 (2021).
[26] K. Marchais, J. Girardot, C. Metton, I. Iordanoff, A 3D DEM simulation to study the influence of material and process parameters on spreading of metallic powder in additive manufacturing, Comput. Part. Mech. 8 (2021) 943–953.
[27] L. Si, T. Zhang, M. Zhou, M. Li, Yun Zhang, H. Zhou, Numerical simulation of the flow behavior and powder spreading mechanism in powder bed-based additive manufacturing, Powder Technol. 394 (2021) 1004–1016.
[28] T. Cheng, H. Chen, Q. Wei, The role of roller rotation pattern in the spreading process of polymer/short-fiber composite powder in selective laser sintering, Polymers (Basel) 14 (2022).
[29] L. Cordova, T. Bora, M.D. Smitb, M. Camposc, T. Tingaa, Measuring the spreadability of pre-treated and moisturized powders for laser powder bed fusion, Addit. Manuf. 32 (2020) 101082.
[30] H. Chen, T. Cheng, Q. Wei, W. Yan, Dynamics of short fiber/polymer composite particles in paving process of additive manufacturing, Addit. Manuf. 47 (2021).
[31] S. Beitz, R. Uerlich, T. Bokelmann, A. Diener, T. Vietor, A. Kwade, Influence of powder deposition on powder bed and specimen properties, Materials (Basel) 12 (2019).
[32] S.T.T. De Silva, C. Doblin, S. Gulizia, I. Cole, R.J. Toh, Assessing the feasibility of using an irregularly shaped ta and spherical Ti bimodal powder blend on the powder spreadability process in powder bed fusion systems, Powder Technol. 428 (2023).
[33] D. Oropeza, R.W. Penny, D. Gilbert, A.J. Hart, Mechanized spreading of ceramic powder layers for additive manufacturing characterized by transmission x-ray imaging: influence of powder feedstock and spreading parameters on powder layer density, Powder Technol. 398 (2022).
[34] M. Lupo, S.Z. Ajabshir, D. Sofia, D. Barletta, M. Poletto, Experimental metrics of the powder layer quality in the selective laser sintering process, Powder Technol. 419 (2023) 118346.
[35] T.-P. Le, X. Wang, K.P. Davidson, J.E. Fronda, M. Seita, Experimental analysis of powder layer quality as a function of feedstock and recoating strategies, Addit. Manuf. 39 (2021) 101890.
[36] S. Haeri, Y. Wangb, J.S.O. Ghitab, Discrete element simulation and experimental study of powder spreading process in additive manufacturing, Powder Technol. 306 (2016) 45–54.
[37] Y. He, Jabbar Gardy, Ali Hassanpour, A.E. Bayly, A digital-based approach for characterising spread powder layer in additive manufacturing, Mater. Des. 196 (2020) 109102.
[38] E.J.R. Parteli, T. Pöschel, Particle-based simulation of powder application in additive manufacturing, Powder Technol. 288 (2016) 96–102.
[39] L.I. Escano, N.D. Parab, L. Xiong, Q. Guo, C. Zhao, K. Fezzaa, W. Everhart, T. Sun, L. Chen, Revealing particle-scale powder spreading dynamics in powderbed-based additive manufacturing process by high-speed x-ray imaging, Sci. Rep. 8 (2018) 15079.
[40] S. Yim, H. Bian, K. Aoyagi, K. Yamanaka, A. Chiba, Spreading behavior of Ti 48Al 2Cr 2Nb powders in powder bed fusion additive manufacturing process: experimental and discrete element method study, Addit. Manuf. 49 (2022).
[41] Standard Guide for Additive Manufacturing of Metals — Feedstock Materials — Assessment of Powder Spreadability, ASTM F3522-22, 2023.
[42] S. Wu, Z. Lei, M. Jiang, J. Liang, B. Li, Y. Chen, Experimental investigation and discrete element modeling for particle-scale powder spreading dynamics in powder-bed-fusion-based additive manufacturing, Powder Technol. 403 (2022) 117390.
[43] J. Zhang, Y. Tan, T. Bao, Y. Xu, X. Xiao, S. Jiang, Discrete element simulation of the effect of roller-spreading parameters on powder-bed density in additive manufacturing, Materials 13 (2020) 2285.
[44] L. Cao, Study on the numerical simulation of laying powder for the selective laser melting process, Int. J. Adv. Manuf. Technol. 105 (2019).
[45] M. Mehrabi, J. Gardy, F.A. Talebi, A. Farshchi, A. Hassanpour, A.E. Bayly, An investigation of the effect of powder flowability on the powder spreading in additive manufacturing, Powder Technol. 413 (2023) 117997.
[46] Z. Haydari, The Spreading Behaviour of Stainless Steel Powders for Additive Manufacturing, Doctoral dissertation, University of Leeds, 2021.
[47] W. Nan, Y. Gu, Experimental investigation on the spreadability of cohesive and frictional powder, Adv. Powder Technol. 33 (2022) 103466.
[48] W. Nan, M. Pasha, U. Zafar, S. Nadimi, W.P. Goh, M. Ghadiri, Characterisation of gas-atomised metal powders used in binder jet 3D printing, Powder Technol 436 (2024) 119471.
[49] S. Zinatlou Ajabshir, D. Sofia, C. Hare, D. Barletta, M. Poletto, Experimental characterisation of the spreading of polymeric powders in powder bed fusion additive manufacturing process at changing temperature conditions, Adv. Powder Technol. 35 (2024).
[50] C. Vakifahmetoglu, B. Hasdemir, L. Biasetto, Spreadability of metal powders for laser-powder bed fusion via simple image processing steps, Materials (Basel) 15 (2021).
[51] A.B. Spierings, M. Voegtlin, T. Bauer, K. Wegener, Powder flowability characterisation methodology for powder-bed-based metal additive manufacturing, Progr. Addit. Manufact. 1 (2016) 9–20.
[52] E.R.L. Espiritu, A. Kumar, A. Nommeots-Nomm, J.A.M. Lerma, M. Brochu, Investigation of the rotating drum technique to characterise powder flow in controlled and low pressure environments, Powder Technol. 366 (2020) 925–937.
[53] D. Ruggi, M. Lupo, D. Sofia, C. Barrès, D. Barletta, M. Poletto, Flow properties of polymeric powders for selective laser sintering, Powder Technol. 370 (2020) 288–297.
[54] J. Zegzulka, D. Gelnar, L. Jezerska, R. Prokes, J. Rozbroj, Characterization and flowability methods for metal powders, Sci. Rep. 10 (2020) 21004.
[55] U. Zafar, C. Hare, A. Hassanpour, M. Ghadiri, Ball indentation on powder beds for assessing powder flowability: analysis of operation window, Powder Technol. 310 (2017) 300–306.
[56] W. Nan, M. Ghadiri, Numerical simulation of powder flow during spreading in additive manufacturing, Powder Technol. 342 (2019) 801–807.
[57] H. Chen, Y. Chen, Y. Liu, Q. Wei, Y. Shi, W. Yan, Packing quality of powder layer during counter-rolling-type powder spreading process in additive manufacturing, Int. J. Mach. Tools Manuf. 153 (2020).
[58] L. Wang, Z. Zhou, E. Li, H. Shen, A. Yu, Powder deposition mechanism during powder spreading with different spreader geometries in powder bed fusion additive manufacturing, Powder Technol. 395 (2022) 802–810.
[59] J. Wang, D. Yao, M. Li, X. An, S. Li, W. Hou, X. Zhang, G. Yang, J. Wang, L. Wang, Hierarchical effects of multi-layer powder spreading in the electron beam powder bed fusion additive manufacturing of pure tungsten material, Addit. Manuf. 55 (2022).
[60] D. Yao, X. Liu, J. Wang, W. Fan, M. Li, H. Fu, H. Zhang, X. Yang, Q. Zou, X. An, Numerical insights on the spreading of practical 316 L stainless steel powder in SLM additive manufacturing, Powder Technol. 390 (2021) 197–208.
[61] Y. Lee, A.K. Gurnon, D. Bodner, S. Simunovic, Effect of particle spreading dynamics on powder bed quality in metal additive manufacturing, integrating materials and manufacturing, Innovation 9 (2020) 410–422.
[62] C. Meier, R. Weissbach, J. Weinberg, W.A. Wall, A.J. Hart, Critical influences of particle size and adhesion on the powder layer uniformity in metal additive manufacturing, J. Mater. Process. Technol. 266 (2019) 484–501.
[63] Q. Wu, C. Qiao, D. Yao, X. An, H. Zhang, H. Fu, X. Yang, Q. Zou, Research on improving the spreadability of viscous powder in additive manufacturing, Powder Technol. 413 (2023).
[64] Y.M. Fouda, A.E. Bayly, A DEM Study of Powder Spreading in Additive Layer Manufacturing, Springer, 2019.
[65] D. Schiochet Nasato, T. Pöschel, Influence of particle shape in additive manufacturing: discrete element simulations of polyamide 11 and polyamide 12, Addit. Manuf. 36 (2020).
[66] R.W. Penny, D. Oropeza, P.M. Praegla, R. Weissbach, C. Meier, W.A. Wall, A. John Hart, Quantitative analysis of thin metal powder layers via transmission X-ray imaging and discrete element simulation: Blade-based spreading approaches, Powder Technol. (2024) 432.
[67] M. Stephan, G. Roux, A. Burr, C. Ablitzer, J.-P. Garandet, Identification of the influential DEM contact law parameters on powder bed quality and flow in additive manufacturing configurations, Powder Technol. 429 (2023).

[68] Y. Yu, T. Ma, S. Wang, M. Jiang, S. Gao, Y. Guo, T. Jiang, B.S. Doumbia, B. Yan, S. Shen, Study on the powder-spreading process of walnut Shell/co-PES biomass composite powder in additive manufacturing, Materials (Basel) 16 (2023).
[69] U. Habiba, R.J. Hebert, Powder spreading mechanism in laser powder bed fusion additive manufacturing: experiments and computational approach using discrete element method, Materials (Basel) 16 (2023).
[70] H. Chen, Q. Wei, Y. Zhang, F. Chen, Y. Shi, W. Yan, Powder-spreading mechanisms in powder-bed-based additive manufacturing: experiments and computational modeling, Acta Mater. 179 (2019) 158–171.
[71] L. Wang, E. Li, Z. Zhou, B. Zhang, A. Yu, Simulation of powder spreading of functionally graded materials in powder bed fusion additive manufacturing, Acta Mech. Sinica 39 (2023).
[72] W. Nan, M. Pasha, M. Ghadiri, Numerical simulation of particle flow and segregation during roller spreading process in additive manufacturing, Powder Technol. 364 (2020) 811–821.
[73] J. Zhang, Y. Tan, X. Xiao, S. Jiang, Comparison of roller-spreading and blade-spreading processes in powder-bed additive manufacturing by DEM simulations, Particuology 66 (2022) 48–58.
[74] L. Wang, E.L. Li, H. Shen, R.P. Zou, A.B. Yu, Z.Y. Zhou, Adhesion effects on spreading of metal powders in selective laser melting, Powder Technol. 363 (2020) 602–610.
[75] R.W. Penny, D. Oropeza, R. Weissbach, P.M. Praegla, C. Meier, W.A. Wall, A. J. Hart, Quantitative analysis of thin metal powder layers via transmission X-ray imaging and discrete element simulation: roller-based spreading approaches, Powder Technol. 432 (2024).
[76] W. Nan, M. Pasha, M. Ghadiri, Effect of gas-particle interaction on roller spreading process in additive manufacturing, Powder Technol. 372 (2020) 466–476.
[77] Z. Li, M. Mizutani, Influence of layer thickness and substrate bed on the void fraction of powder layers for laser powder bed fusion, Powder Technol. 418 (2023).
[78] S. Khajepor, O. Ejtehadi, S. Haeri, The effects of interstitial inert gas on the spreading of Inconel 718 in powder bed fusion, Addit. Manuf. 75 (2023).
[79] U. Zafar, C. Hare, A. Hassanpour, M. Ghadiri, Drop test: a new method to measure the particle adhesion force, Powder Technol. 264 (2014) 236–241.
[80] L. Pedrolli, S. Nadimi, B. Achiaga, A. López, Estimation of mesoscale surface energy in the kinetic adhesion test, Powder Technol. 435 (2024).
[81] W. Nan, L. Ge, W. Xuan, Y. Gu, Transient jamming of granular flow by blade spreading, Powder Technol. 431 (2024).
[82] D. Schiochet Nasato, H. Briesen, T. Pöschel, Influence of vibrating recoating mechanism for the deposition of powders in additive manufacturing: discrete element simulations of polyamide 12, Addit. Manuf. 48 (2021).
[83] H. Chen, W. Zhu, H. Tang, W. Yan, Oriented structure of short fiber reinforced polymer composites processed by selective laser sintering: the role of powder-spreading process, Int. J. Mach. Tools Manuf. 163 (2021).
[84] K. Johnson, K. Kendall, A. Roberts, Surface energy and the contact of elastic solids, Proc. Roy. Soc. Lond. A 324 (1971) 301–313.
[85] X. Chen, J.A. Elliott, On the scaling law of JKR contact model for coarse-grained cohesive particles, Chem. Eng. Sci. 227 (2020) 115906.
[86] M.A. Behjani, N. Rahmanian, N. Fardina Bt Abdul Ghani, A. Hassanpour, An investigation on process of seeded granulation in a continuous drum granulator using DEM, Adv. Powder Technol. 28 (2017) 2456–2464.
[87] M.J. Khala, C. Hare, C.-Y. Wu, N. Venugopal, M.J. Murtagh, T. Freeman, Rheological response of granular materials under dynamic conditions, Powder Technol. 398 (2022).
[88] Y. He, A. Hassanpour, A.E. Bayly, Combined effect of particle size and surface cohesiveness on powder spreadability for additive manufacturing, Powder Technol. 392 (2021) 191–203.
[89] Y. He, A. Hassanpour, A.E. Bayly, Linking particle properties to layer characteristics: discrete element modelling of cohesive fine powder spreading in additive manufacturing, Addit. Manuf. 36 (2020).
[90] S. Zinatlou Ajabshir, C. Hare, D. Sofia, D. Barletta, M. Poletto, Investigating the effect of temperature on powder spreading behaviour in powder bed fusion additive manufacturing process by Discrete Element Method, Powder Technol. (2024) 436.
[91] H. Chen, Q. Wei, S. Wen, Z. Li, Y. Shi, Flow behavior of powder particles in layering process of selective laser melting: numerical modeling and experimental verification based on discrete element method, Int. J. Mach. Tools Manuf. 123 (2017) 146–159.
[92] M. Upadhyay, T. Sivarupan, M. El Mansori, 3D printing for rapid sand casting—a review, J. Manuf. Process. 29 (2017) 211–220.
[93] Y. Xu, L. Ge, W. Nan, Investigation on the spreading behaviour of sand powder used in binder jet 3D printing, Granul. Matter 26 (2024).
[94] Z. Zhou, F. Buchanan, C. Mitchell, N. Dunne, Printability of calcium phosphate: calcium sulfate powders for the application of tissue engineered bone scaffolds using the 3D printing technique, Mater. Sci. Eng. C Mater. Biol. Appl. 38 (2014) 1–10.
[95] S. Spath, H. Seitz, Influence of grain size and grain-size distribution on workability of granules with 3D printing, Int. J. Adv. Manuf. Technol. 70 (2013) 135–144.
[96] Y. Ma, T.M. Evans, N. Philips, N. Cunningham, Numerical simulation of the effect of fine fraction on the flowability of powders in additive manufacturing, Powder Technol. 360 (2020) 608–621.
[97] Y.S. Lee, P. Nandwana, W. Zhang, Dynamic simulation of powder packing structure for powder bed additive manufacturing, Int. J. Adv. Manuf. Technol. 96 (2018) 1507–1520.
[98] H. Salehi, J. Cummins, E. Gallino, V. Garg, T. Deng, A. Hassanpour, M. Bradley, Optimising spread-layer quality in powder additive manufacturing: assessing packing fraction and segregation tendency, Processes 11 (2023).
[99] J. Zhang, N. Wang, X. Chen, Y. Tan, Particle gradations optimization for powder spreading in additive manufacturing, Mater. Des. 236 (2023).
[100] P. Yadav, O. Rigo, C. Arvieu, E. Le Guen, E. Lacoste, Data treatment of in situ monitoring systems in selective laser melting machines, Adv. Eng. Mater. 23 (2021).
[101] L. Scime, D. Siddel, S. Baird, V. Paquit, Layer-wise anomaly detection and classification for powder bed additive manufacturing processes: a machine-agnostic algorithm for real-time pixel-wise semantic segmentation, Addit. Manuf. 36 (2020).
[102] F.G. Fischer, M.G. Zimmermann, N. Praetzsch, C. Knaak, Monitoring of the powder bed quality in metal additive manufacturing using deep transfer learning, Mater. Des. 222 (2022).
[103] L. Ge, R. Xu, W. Nan, Wear of blade spreader during powder spreading in additive manufacturing, Tribol. Int. 188 (2023).
[104] P.S. Desai, C.F. Higgs, Spreading process maps for powder-bed additive manufacturing derived from physics model-based machine learning, Metals 9 (2019).
[105] J.L. Bartlett, A. Jarama, J. Jones, X. Li, Prediction of microstructural defects in additive manufacturing from powder bed quality using digital image correlation, Mater. Sci. Eng. A 794 (2020).
[106] M.A. Ansari, A. Crampton, S. Parkinson, A layer-wise surface deformation defect detection by convolutional neural networks in laser powder-bed fusion images, Materials (Basel) 15 (2022).
[107] L. Scime, J. Beuth, A multi-scale convolutional neural network for autonomous anomaly detection and classification in a laser powder bed fusion additive manufacturing process, Addit. Manuf. 24 (2018) 273–286.
[108] L. Scime, J. Beuth, Anomaly detection and classification in a laser powder bed additive manufacturing process using a trained computer vision algorithm, Addit. Manuf. 19 (2018) 114–126.
[109] Y. Wu, M. Li, J. Wang, Y. Wang, X. An, H. Fu, H. Zhang, X. Yang, Q. Zou, Powder-bed-fusion additive manufacturing of molybdenum: process simulation, optimization, and property prediction, Addit. Manuf. 58 (2022).
[110] S. Haeri, Optimisation of blade type spreaders for powder bed preparation in additive manufacturing using DEM simulations, Powder Technol. 321 (2017) 94–104.
[111] A. Phua, C. Doblin, P. Owen, C.H.J. Davies, G.W. Delaney, The effect of recoater geometry and speed on granular convection and size segregation in powder bed fusion, Powder Technol. 394 (2021) 632–644.
[112] Q. Wu, C. Qiao, J. Wang, D. Yao, Y. Wu, W. Fan, M. Li, X. An, Adaptability investigations on bottom modified blade in powder spreading process of additive manufacturing, Addit. Manuf. 49 (2022).